Summer 7-25-2023

Adaptive GPS Antenna Array Beam Nulling Effectiveness Under Varying Antenna Element Positioning

Aadesh Neel
University of New Mexico - Main Campus

Aadesh Neel

Candidate

Electrical and Computer Engineering

Department

This thesis is approved, and it is acceptable in quality and form for publication:

Approved by the Thesis Committee:

Christos Christodoulou, Chairperson

Jeffery Williams

Mark Gilmore

ADAPTIVE ANTENNA ARRAY BEAMNULLING UNDER VARYING ANTENNA ELEMENT POSITIONING

BY

AADESH NEEL

BACHELOR'S OF SCIENCE IN ELECTRICAL ENGINEERING

THESIS

Submitted in Partial Fulfillment of the
Requirements for the Degree of

Masters of Science
Electrical Engineering

The University of New Mexico
Albuquerque, New Mexico

July 2023

Acknowledgements

I would like to thank Dr. Jeffery Williams for his constant support, encouragement, and guidance throughout the last few years of my research and studies. Without him or his effortless work at Sandia National Labs, this project would not have been conceived.

I would like to thank Professor Christos Christodoulou for the countless resources and explanations he provided in order to achieve these results. I am also thankful to everybody at the Antennas and RF lab for creating a positive work environment and making it a joy to come in and work.

I would like to thank David Gardner for the encouraging words of support, interfacing with Sandia, and providing the career experience and guidance that lead me to this work.

I would also like to thank everybody in the Directed Energy Enterprise. The people in this group helped me discover my passion for applied electromagnetics and provided countless hours of experience and explanations in the exceptional work we performed at SNL. Without them, I would not have had the knowledge to complete this work.

Finally, I would like to thank all my family and friends. They have truly supported and guided through my education, and I would not be here without them.

ADAPTIVE ANTENNA ARRAY BEAMNULLING UNDER VARYING ANTENNA ELEMENT POSITIONING

BY

AADESH NEEL

B.S., ELECTRICAL ENGINEERING, THE UNIVERSITY OF NEW MEXICO, 2020

M.S., ELECTRICAL ENGINEERING, THE UNIVERSITY OF NEW MEXICO, 2023

ABSTRACT

Global Positioning System (GPS) is an essential part of modern life but is susceptible to same frequency jamming. GPS jamming can add excessive noise to a received low power signal and have the capability to change or completely distort information being sent through the GPS signal. Adaptive antenna arrays have long since been a solution to mitigating GPS jamming via beamnulling algorithms. However, there is little research on the effectiveness of these beamnulling algorithms under varying element positioning. In this work, an adaptive antenna array, consisting of Right-Hand Circularly Polarized (RHCP) nearly square GPS antenna elements, was constructed and tested for beamnulling applications. Two beamnulling algorithms (LCMV and MVDR) and two orientations (Orientation 1, an optimal 2x2 $\lambda/2$ spacing orientation, and Orientation 2, a less common "+" shaped array with 0.55λ spacing) are simulated, tested, and compared with each other.

CONTENTS

LIST OF FIGURES

LIST OF TABLES

GLOSSARY

ADC – Analog to Digital Converter

BPS – Bits Per Second

BPSK – Binary Phase Shift Keying

C/A-Code – Course Acquisition Code

CP – Circular Polarization

CW – Continuous Wave

DoA – Direction of Arrival

GNSS – Global Navigation Satellite System

GPS – Global Positioning System

INR – Interference to Noise Ratio

L1 – Link 1

L2 – Link 2

L5 – Link 5

LCMV – Linearly Constrained Minimum Variance

LHCP – Left Hand Circular Polarization

M-Code – Military Code

MUSIC – MUltiple SIgnal Classification

MVDR – Minimum Variance Distortionless Response

PRN Code– Pseudo Random Noise Code

RF – Radio Frequency

RHCP – Right Hand Circularly Polarized

SDR – Software Defined Radio

SNR – Signal to Noise Ration

VSWR – Voltage Standing Wave Ratio

1. INTRODUCTION

GPS (global positioning system) is essential for navigation and tracking not only for military and defense applications, but also for civilian and commercial applications. With that in mind, it is important to acknowledge that, just like any wireless communication system, GPS is vulnerable to electronic interference, whether it be accidental, or due to electronic warfare. As a result, many mitigation tactics involving receiving antennas are implemented in order to ensure robust and uninterrupted communication with GPS signals. These mitigation tactics have a big presence in industry and are a well-established research topic. One such tactic is the use of adaptive antenna arrays (smart antennas) in order to "null" out the jamming and/or spoofing signal that can interrupt communication with GPS. This is a practice known as beamnulling, or more generally beamforming. This is mainly done using various signal processing algorithms that can change the received signals to only keep the GPS information while simultaneously throwing out the jamming or spoofing information via manipulating the antenna array's radiation pattern. However, there is very little literature describing how the positioning of the antenna elements in an adaptive array affects these anti-jam beam nulling algorithms. The work developed in this thesis is a joint effort between The University of New Mexico's Antennas and RF Labs and Sandia National Labs in order to better understand how the positioning of antenna elements effects general beam nulling algorithms.

In this thesis, two adaptive antenna arrays were designed for GPS purposes. They differed in element spacing and were tested in an environment with a target GPS frequency signal and a CW (continuous wave) jamming signal at the same frequency. Frist array (orientation 1) was a simple 4 element planar array with optimal $\lambda/2$ spacing, while the second array (orientation 2) was a less

common "+" shaped array with 0.55λ spacing. Furthermore, two different beam nulling algorithms were tested: the LCMV algorithm and the MVDR algorithm. The question posed here is: **Which orientation (Orientation 1 or Orientation 2) and which beam nulling algorithm (MVDR or LCMV) is most effective in a beam nulling adaptive scenario?** The PSD (power spectral density) was recorded for each orientation without beam nulling and with each beam nulling algorithm applied. The cancellation is calculated and used as a figure of merit for the effectiveness of each orientation and algorithm combination.

2. GPS Architecture

This chapter provides some introductory material about GPS in the form of a literature review. This includes the GPS architecture, the GPS signal creation process, and a general structure for GPS receivers.

GPS is the most widely available GNSS in use today. Although it was developed in the 1970's, GPS is certainly a necessity in the modern age due to its many practical uses for both military and civilian applications. The free availability of this technology has enhanced many applications, which include aviation, public safety, recreation, telecommunications, transportation, mapping and surveying activities, financial systems, and electric power networks. There are three components that make up a GPS signal: An RF carrier frequency, a PRN code, and an encoded navigation message originated from a GPS satellite. This section will go over each of the three components that make up GPS.

2.1: GPS satellites and Navigation Message.

The creation and transmission of GPS signals is done onboard a GPS satellite. GPS is not to be confused with Global Navigation Satellite System, or GNSS. GNSS is a blanket term that encompasses all satellite navigation systems created by every country. Other satellite systems

include BeiDou (China), Galileo (Europe), and GLONASS (Russia). These other satellite systems work on the same theory as GPS but use different satellites and different software communication systems. It is worth noting that GPS was the first GNSS and paved the way for all the others. Currently, there are 31 dedicated GPS satellites orbiting earth and there are plans to launch even more advanced satellites with additional transmitting capabilities. Information is encoded onto a GPS carrier frequency using the various encoding techniques discussed in Section 2.2. This creates the navigation message. The navigation message is 50 bps binary data (+1 or -1) that contains the satellite almanac data the ephemeris data of the satellite, and the time information when the message was sent, which is all pertinent to the location and navigation solutions provided by GPS receivers [1]. Almanac data allows for the computation of the position of all satellites in the constellation, admittedly with a reduced accuracy (1 - 2 km of 1-sigma error), which is needed for the acquisition of the signal by the receiver. Ephemeris parameters are needed to compute the satellite coordinates with enough accuracy. The time parameters include a time stamp the message was sent and clock correction in order to compute satellite clock offsets and time conversions. The ephemeris and clock parameters are usually updated every two hours, while the almanac data is updated at least every six days. It is also worth noting that service parameters are included in order to identify and monitor the health of that satellite. Furthermore, ionospheric parameters are included in order to model the signal transmission for even more accuracy.

Location data using GPS signals works based on the concept of trilateration [2]. The equations used for a trilateration of a GPS signal are as follows:

$$\sqrt{(x-A_1)^2+(y-B_1)^2+(z-C_1)^2} = c(t_1-d)$$

$$\sqrt{(x-A_2)^2+(y-B_2)^2+(z-C_2)^2} = c(t_2-d)$$

$$\sqrt{(x-A_3)^2+(y-B_3)^2+(z-C_3)^2} = c(t_3-d)$$

$$\sqrt{(x-A_4)^2+(y-B_4)^2+(z-C_4)^2} = c(t_4-d)$$

Equations 2.1

Equations 2.1 above are the equations that solve for the current position of the asset being tracked by GPS. An, Bn, Cn are the spatial coordinates of the n satellite being tracked, tn is the travel time for the signal to reach the receiver from the satellite, (x,y,z) are the spatial coordinates (Cartesian) for the asset being tracked, and d is the difference in time between the receivers clock and the satellites atomic clock, which can also be thought of as the clock offset. To track the current location of the phone and provide the best directions, these equations are continuously solved for x,y,z and d. The d value is needed because the location of the receiver is approximated using the travel time from the satellite to the receiver. Otherwise, there would be small errors caused by a time mismatches between the satellite clock and the system clock, resulting in spatial coordinate errors of the receiver. In order to solve these equations, the ephemeris data and clock status of each satellite being tracked will need to be known. This information is easily obtainable from the GPS message being sent. As mentioned earlier, all ephemeris data is encoded on the signal. In all cases, 4 GPS satellites will need to be tracked to solve for the 4 unknowns in the equations above, (i.e., x, y, z, d). In order to solve these equations two primary methods are used: The first is solving 4 equations for the 4 unknowns by using the quadratic formula. However, this method yields two solutions. As a result, the second method is preferred. The second method is a multivariate Newton method where an initial guess is made and then iterated until an answer is

guessed. This method is not computationally rigorous and the correct answer usually converges in about 20 iterations. All the computation is done at the receiver end.

2.2: GPS RF Carrier Frequencies

GPS transmits in three L-band carrier frequencies. These three carrier frequencies, or colloquially known as "links," are L1 (1547.52 MHz), L2 (1227.60 MHz), and L5 (1176.45 MHz). All GPS signals are RHCP (Right Hand Circularly Polarized.) This means that a receiving GPS antenna would need be RHCP as well or there will be a 3 dB power loss. It is worth mentioning that L5 is a new carrier frequency that is currently being implemented into new GPS satellites. The L-band was initially chosen for multiple reasons. Firstly, not many systems in the 1970's, when the GPS was first developed, transmitted at L-band because it was considered to be high frequency. Furthermore, the L-band is generally unaffected by weather and the ionospheric delays are manageable. Finally, directional antennas are not needed when dealing with the L-band. Since the use of L2 is reserved for military purposes and the fact that L5 is a relatively new frequency, the only signal being studied in this thesis is L1. In order to encode GPS information, which is known as the navigation message onto the carrier frequency (L1), a modulation technique known as BPSK (binary phase shift keying) is used. In BPSK modulation, binary data that comprises the sum of the navigation message and the PRN code, which will be discussed in the next section, are encoded through a phase shift. Whenever a phase shift of 180 degrees occurs, the value is switched from a high to a low or vice versa. This modulation method works because GPS signals are fairly short binary codes with values of either -1 or +1.

2.3: PRN codes

A PRN code (pseudo-random-noise-code) is a deterministically created binary code that has a spectrum similar to random noise, although it is not actually random noise. Since the

navigation message is a baseband signal, PRN codes have a spread-out spectrum so that the bandwidth of the transmitted signal becomes significantly wide after the navigation code and the PRN are summed together. Each PRN code has a “chipping rate.” This is the number of chips (bits) per second being transmitted. Furthermore, each satellite has a different PRN code, and that is how we can differentiate between each satellite. Each GPS receiver will replicate each PRN code for each satellite and correlate the incoming signal to its replica. Depending on the auto-correlation and cross-correlation properties, we can effectively tell which satellite sent the signal. This is discussed more at the end of this section. For L1 there are multiple PRN coding techniques used simultaneously. Civilians have access to a PRN coding technique called C/A (Course Acquisition) code, in which the length of the code is 1023 chips and transmission chipping rate of 1.023Mchips/s. The navigation message of 50 bps is then summed and therefore modulated into the PRN code to create a new bitstream. Finally, that bit stream is BPSK modulated onto the carrier frequency (either L1, L2, or L5)

The military and the Department of Defense have access to two extra PRN codes: P[Y] code (an anti-spoofing version of Y-code), and the newly created M-Code. Just as with L2, these codes are only for military use, and a lot of information is not known to civilians, like their code length, their code rate, or their modulation technique, so they will not be discussed in this work. Figure 2.1 below above summarizes describes the generation of the transmitted GPS signal.

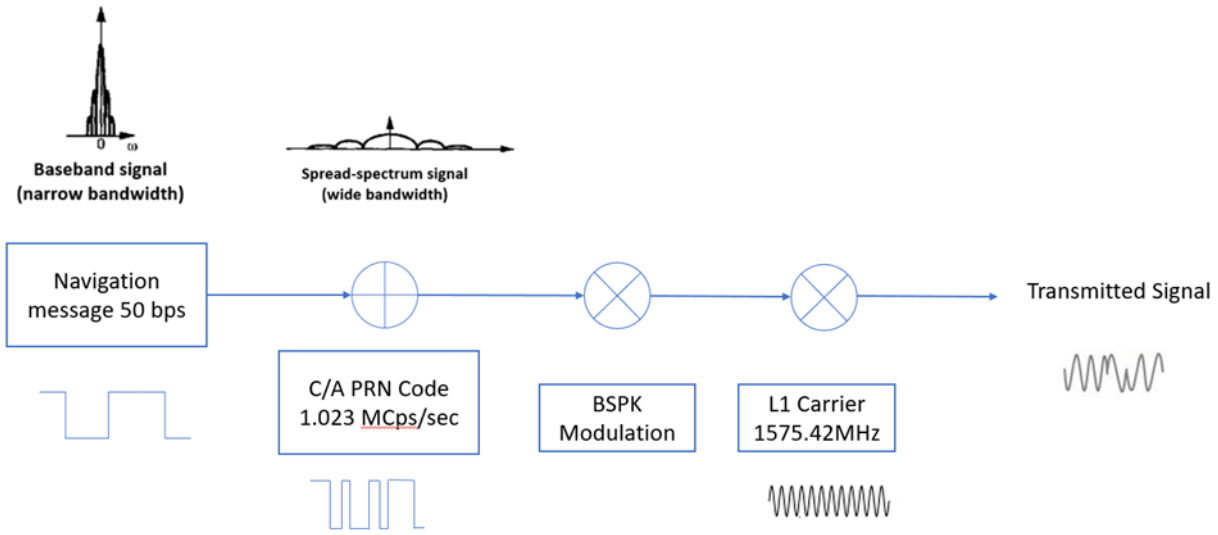

Figure 2-1: GPS Signal Generation Process

In order for a GPS receiver to extract information from the GPS signal, it must perform a correlation operation. The C/A PRN code has generally good cross correlation properties. Table 1 shows some cross correlation properties of the C/A code. C/A code u However, the cross correlation and autocorrelation properties of GPS signals are outside the scope of this work. More information can be found in the review by Glennon and Dempster [3]

Code Length [L]	N	Normalized cross correlation levels	Probability of level
$L = 2^N - 1$	N is even and n is not a multiple of 4	$-[2^{(n+1)/2}+1]/L$	0.25
		-1/L	0.5
		$[2^{(n+1)/2}+1]/L$	0.25
L = 1023 (GPS case)	N = 10	-65/1023	0.125
		-1/1023	0.75
		63/1023	0.125

Table 1: Cross correlation properties of C/A Code

To summarize, PRN codes are pseudorandom noise sequences used in GPS for satellite identification, signal modulation/demodulation, time synchronization, and acquiring and tracking satellite signals.

3. ADAPTIVE ANTENNA ARRAYS AND ADAPTIVE ALGORITHMS LITERATURE REVIEW

This chapter focuses on some basic techniques and literature review regarding adaptive antennas (also known as smart antennas) and adaptive arrays, their front end, the various beamforming algorithms used to null out signals of interest, and DoA estimation algorithms.

3.1: Adaptive Array Front End Receiver Architecture

An adaptive antenna array front-end architecture refers to a system that uses an array of antennas to receive and process signals in a way that improves overall system performance. It is

commonly used in wireless communication systems, such as cellular networks, radar systems, and wireless sensor networks.

The main objective of an adaptive antenna array is to enhance the quality of received signals by suppressing interference and improving the signal-to-noise ratio (SNR). This is achieved by exploiting the spatial diversity offered by multiple antennas and employing adaptive signal processing algorithms.

Figure 3-1 is a block diagram of a general GPS adaptive array front end. Here are the key components:

1. **Antennas:** The signal is received by multiple antennas that are optimally spaced away from each other.
2. **RF/IF converter**: Next, the antenna is then connected to a general super-heterodyne RF/IF converter front-end that includes components such as low-noise amplifiers (LNAs), filters, mixers, and frequency synthesizers. These components are responsible for amplifying, filtering, and down converting the received signals.
3. **ADC:** The received signals from the antennas are converted into digital form by an analog to digital converter (ADC) and processed using DSP techniques. This includes filtering, interference cancellation, and other signal processing operations, such as beamforming.
4. **w (weight control):** When the signals are properly digitized, the system manages the adaptive algorithms, weights, and other parameters of the adaptive antenna array.
5. **DAC:** The digital signal is then converted back to analog (DAC).

6. **IF/RF Converter:** The IF is then converted back to RF, and our adaptive signal is created.
7. **GPS Receiver:** Finally, the adaptive signal is fed into a standalone GPS receiver (either commercial or military grade) and the GPS information is extracted.

The adaptive antenna array front-end architecture offers several advantages, including increased signal quality, improved coverage, enhanced capacity, and better resistance to interference. It enables systems to adapt to changing propagation conditions, mitigate multipath fading, and enhance the overall system performance.

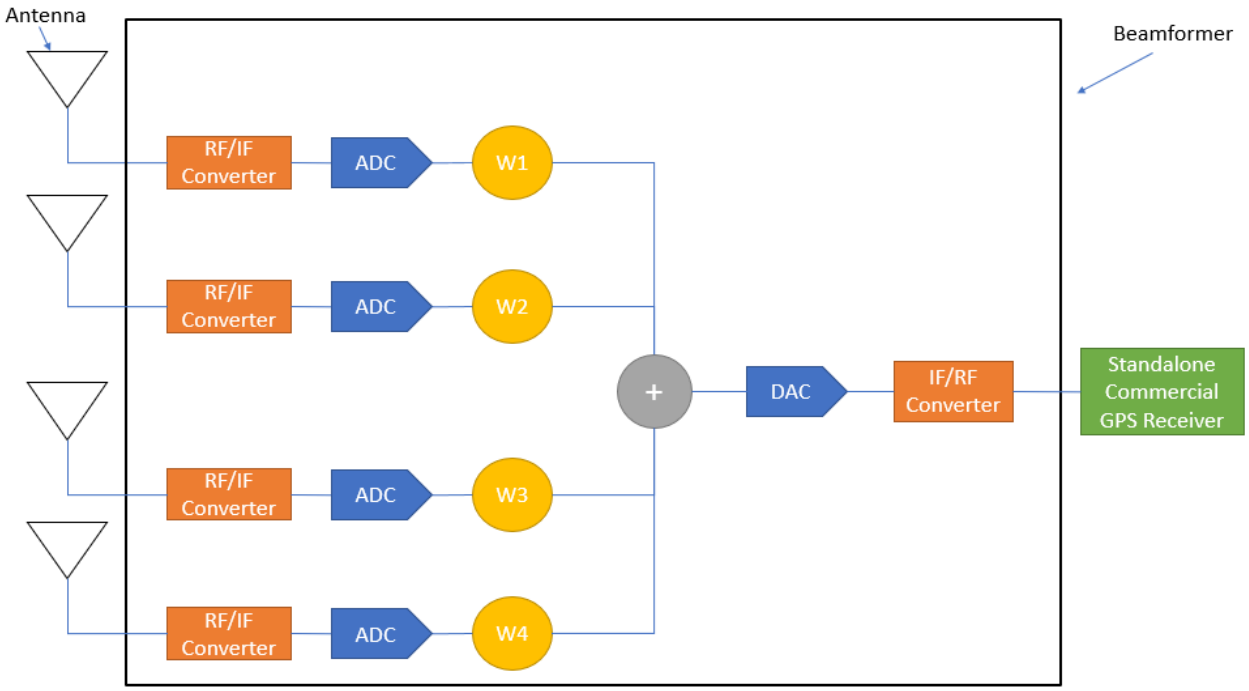

Figure 3-1: Adaptive Array Front End Receiver Architecture

3.2: Adaptive Antenna Array and Beamforming Theory

Adaptive antennas have been part of mainstream antenna research since 1957 where Paul W. Howells invented a method to electronically steer an antennas radiation pattern away from a jammer while working at the General Electric Corporation [4]. In 1962, P.G. Howells and Sidney Applebaum tested a five-loop side-lobe canceller against five jammers. Because of this test, real interest was sparked for their research and eventually lead to Applebaum publishing a paper titled Adaptive Arrays [5] in which he went over the weighting used on the received signals for the correct beamforming. The concept of beamforming refers to a multichannel signal processing technique that amplifies target signals coming from target directions while simultaneously reducing signals coming from other directions. Note that it is possible to beamform with both electromagnetic signals as well as acoustic signals.

Antenna arrays exhibit an effective radiation pattern that is a super position of each of the element's radiation pattern. This can be expressed in terms of the array factor. For a 2D planar array, the array factor can be expressed as [6]:

$$AF_n(\theta,\varphi) = \sum_{n=1}^{N} I_{1n} e^{j(n-1)\varphi_x} \sum_{m=1}^{M} I_{m1} e^{j(m-1)\varphi_y}$$

Equation 3.1

Where:

$\varphi_x = kd_x\sin(\theta)\cos(\varphi) + \beta_x$

$\varphi_y = kd_y\sin(\theta)\cos(\varphi) + \beta_y$

$k = 2\pi/\lambda$

I_{1n} and I_{m1} are the excitation amplitudes of each element. Note that $I_{mn} = I_{1n}I_{m1}$ and if each element is excited the same way, then $I_{mn} = I_o$. Thus equation 3.1 can be simplified as

$$AF_n(\theta,\varphi) = I_o \sum_{n=1}^{N} e^{j(n-1)\varphi_x} \sum_{m=1}^{M} e^{j(m-1)\varphi_y}$$

Equation 3.2

Phases β_x and β_y can be used to steer the beams of the antenna. For example, if the main beam directed along $\theta = \theta_o$ and $\varphi = \varphi_o$ then the phases must be

$\beta_x = kd_x \sin(\theta_o)\cos(\varphi_o)$

$\beta_y = kd_y \sin(\theta_o)\sin(\varphi_o)$

However, we can also express the array factor in terms of the artificial weighting assigned to each element. The derivation is as follows: If we assume that each element in the array has the same radiation pattern, $p(\theta, \varphi)$, the total output radiation pattern of the antenna, $P(\theta, \varphi)$,

expressed by Fenn is [7]:

$$P(\theta,\varphi) = p(\theta,\varphi) \sum_{i=1}^{N} w_i e^{j\left(kdxsin(\theta)cos(\varphi)+kdysin(\theta)sin(\varphi)\right)}$$

Equation 3.3

Consider the portion of equation 3.3 below

$$\sum_{i=1}^{N} w_i e^{j\left(kdxsin(\theta)cos(\varphi)+kdysin(\theta)sin(\varphi)\right)}$$

Equation 3.4

We can see that 3.4 and 3.2 are comparable if you replace the excitation amplitude with the complex weighting factor. This means that by changing the weighting, which is comparable to excitation signal of each element, we can change the array factor, and in turn, the radiation pattern.

Consider a received signal matrix that encompasses all signals being received by an antenna as discussed in [7]

$$\boldsymbol{X}(t) = [X_1(t), X_2(t), \dots X_n(t)]$$

Equation 3.5

Similar to equation 3.3, we can change the received signal by multiplying it by a weight vector:

$$\boldsymbol{y}(t) \; = \; \boldsymbol{w^H}(t)\boldsymbol{X}(t)$$

Equation 3.6

Following [7]. If we look at the expected value of **y** and substitute in equation 3.6 we get

$$E|\boldsymbol{y}(t)|^2 = E|\boldsymbol{y}^*(t)\boldsymbol{y}(t)| \; = \; \boldsymbol{w^H R w}$$

Equation 3.7

Where **R**, is the covariance matrix, is mathematically defined as:

$$\boldsymbol{R} \; = \; E|\boldsymbol{X}(t)\boldsymbol{X^H}(t)|$$

Equation 3.8

One useful property of R is that is a Hermitian matrix meaning that it can be decomposed into eigenspace via the spectral theorem.

$$R = \sum_{k=1}^{N} \lambda_k e_k {e_k}^H$$

Equation 3.9

In 3.9 and λ_k is the kth eigenvalue e_k is the kth eigenvector. It is then possible to derive the Applebaum-Howells steady state adapted weight equation in eigenspace. For this general nulling processor, the time dependent adaptive weight equation is given by [7]

$$\tau_o \frac{dw_a}{dt} + [I + \mu R] w_a = w_o$$

Equation 3.10

In this case we define w_o as the quiescent weights (weights before adaptation) and w_a as the adaptive weights. τ_o is a filter time constant, I is the identity matrix. μ is the effective loop gain that provides the threshold for sensing signals. Under steady state conditions, the time derivative can be set to zero, and solving for the adaptive weights yields.

$$[I + \mu R]^{-1} w_o = w_a$$

In order to prevent a situation where the adaptive antenna turns off to reduce nulling, assume that the weights can be normalized to [7]

$$\boldsymbol{sum(w) = w1 + w2 + \ldots + wn = 1}$$

The interference to noise ratio can also be defined as

$$\text{INR} = \frac{\boldsymbol{w^H R w}}{\boldsymbol{w^H w}}$$

Equation 3.11

And the cancellation by an adaptive nulling array is defined as the ratio of the INR before and after cancelation.

$$\text{C} = \frac{INR(before\ adaptation)}{INR(after\ adaptation)}$$

Equation 3.12

Equations 3.11 and 3.12 are very important results. They are used to quantitively compare the effectiveness of the results obtained in this thesis

Using 3.9, the steady state adaptive weight equation can be written in terms of the weight vector and the eigen space version of the covariance:

$$[I + \mu \sum_{k=1}^{N} \lambda_k e_k {e_k}^H] w_a = w_a + \mu \sum_{k=1}^{N} \lambda_k e_k < {e_k}^H, w_a > = w_o$$

Equation 3.13

Note that the term $<e_k^H, w_a> = e_k^H w_a$ is a complex scaler. We can take the product of e_l^H where l = 1,2,3,4…N, where N is the number of elements in the array which yields:

$$< e_l{}^H, w_a > + \mu \sum_{k=1}^{N} \lambda_k < e_l{}^H, e_k >< e_k{}^H, w_a > = < e_k{}^H, w_o >$$

Equation 3.14

Since the eigenvectors are orthonormal, meaning that:

$$< e_l{}^H, e_k > = 1 \; for \; K = l$$

$$< e_l{}^H, e_k > = 0 \; for \; k \neq l$$

We can reduce equation 3.14 to:

$$< e_l{}^H, w_a > + \mu\lambda_l < e_l{}^H, w_a > = < e_l{}^H, w_o > \; for \; l = 1,2,3,\ldots,N$$

Equation 3.15

Solving for $<e_k^H, w_a>$ we get:

$$< e_k{}^H, w_a > = \frac{< e_k{}^H, w_o >}{1 + \mu\lambda_k}$$

Equation 3.16

And finally, substituting in 3.16 into 3.13 we get:

$$w_a = w_o - \sum_{k=1}^{N} \frac{\mu\lambda_k}{1 + \mu\lambda_k} < e_k{}^H, w_o > e_k$$

Equation 3.17

Equation 3.17 is a very important result. It shows how the quiescent weight vector is modified in the presence of interference sources. The quantity $<e_k^H, w_o>$ is the projection of the eigenvector e_k on w_o. For values of $\mu\lambda < 1$, which corresponds to weak interference sources, the adaptive weight vector will be relatively unchanged, but for values $\mu\lambda > 1$, it changes more significantly. Finally, we can express the radiation pattern in terms of the adaptive weight vector, w_a, as:

$$P(\theta, \varphi; w) = P_o(\theta, \varphi; w_o) - \sum_{k=1}^{N} \frac{\mu\lambda_k}{1 + \mu\lambda_k} < e_k{}^H, w_o > P_k(\theta, \varphi; w_k)$$

Equation 3.18

In this case, P is the adaptive radiation pattern, Po is the quiescent radiation pattern (equal weights) and Pk is the kth eigenvector radiation pattern. The negative summation essentially removes any projections of interference source eigenvectors that were included in the quiescent weight pattern, which causes the adaptive pattern to have nulls in the direction of interference. This covers the basics of the theory of beam nulling.

We must also examine a way to calculate **R**, which is the covariance of the received signal matrix **X.** Much research has gone into proper covariance estimation and is quite frankly

beyond the scope of this thesis, as it is more into scope of mathematics and statistics. However, we can follow [8].

$$\boldsymbol{R} = \frac{\boldsymbol{X}\boldsymbol{X}'}{m}$$

Equation 3.19

Where m is the number of snapshots in the received signal matrix.

Thus, all the information obtained to adjust the radiation pattern EXCEPT the adaptive weights. The question becomes what weights will create an optimal radiation pattern. In this work, two algorithms were used: the MVDR and the LCMV algorithms. These algorithms were chosen due to the fact that they are extremely effective with a priori knowledge of the direction of jammers (which is a given in the test setup) as well as the fact that they are not computationally taxing. The sections below outline each algorithm in detail.

3.3: The MVDR Beamforming Algorithm

The Minimum Variance Distortionless Response (MVDR) beamforming algorithm, also known as the Capon beamforming algorithm, is a popular technique used in adaptive antenna arrays to achieve spatial filtering and beamforming. It aims to minimize the output power while maintaining a distortionless response to the desired signal.

The MVDR algorithm [9] considers the spatial characteristics of the received signals and adapts the array weights to maximize the signal power while suppressing interference and noise. Unlike the LCMV algorithm, the MVDR algorithm does not impose explicit constraints on the

interference and noise sources. Instead, it directly minimizes the output power subject to a constraint on the desired signal response.

Here's how the MVDR algorithm works:

1. **Array Geometry and Steering Vector:** The MVDR algorithm assumes an array of antennas with known positions and a desired signal arriving from a specific direction. The array geometry and the steering vector, representing the DOA of the desired signal, are essential inputs to the algorithm.
2. **Covariance Matrix Estimation:** The algorithm estimates the covariance matrix of the received signals at the antenna array. The covariance matrix represents the statistical properties of the received signals and is used to calculate the weights for the beamforming. It is worth mentioning that the MVDR algorithm specifically uses the inverse of the estimated covariance matrix, which represents the inverse spatial correlation matrix of the received signals.
3. **Weight Calculation:** The algorithm calculates the optimal weights for the antenna array by multiplying the inverse covariance matrix with the steering vector. This multiplication effectively creates a spatial filter that enhances the desired signal while suppressing interference and noise.
4. **Beamforming and Signal Reconstruction:** Once the optimal weights are obtained, the MVDR algorithm applies these weights to the received signals from the antennas to create a beam that emphasizes the desired signal and attenuates interference and noise. The beamformed signal is then reconstructed for further processing or transmission.

Consider a received signal matrix X that contains all the signals received by a 4 element antenna array and here are “m” number of snapshots collected from each signal:

$$\boldsymbol{X} = [x_1, x_2, \ldots, x_4]$$

Equation 3.20

We can also represent steering vector matrix as:

$$\boldsymbol{a}(\boldsymbol{r}) = e^{-j\boldsymbol{k}\cdot\boldsymbol{r_n}}$$

Equation 3.21

Where $\boldsymbol{k}$ is the wavevector defined as:

$$k = [k_x, k_y, \mathrm{k}_z] = \frac{2\pi}{\lambda}[sin(\theta)cos(\varphi), sin(\theta)sin(\varphi), cos(\varphi)]$$

and r is the cartesian spatial coordinates for each antenna element number n:

$$\boldsymbol{r} = (dx_n\, dy_n\, dz_n)$$

Following [8], we can represent the optimal weights, w, as an optimization problem that is mathematically represented as:

$$min\ \boldsymbol{w^H R w}$$

$$s.t. \quad \boldsymbol{w^H a}(\boldsymbol{r}) = 1$$

Solving the minimization problem yields the solution:

$$\boldsymbol{w_{MVDR}} = \frac{\boldsymbol{R^{-1}a(r)}}{\boldsymbol{a^{-1}}(r)\boldsymbol{R^{-1}a(r)}}$$

Equation 3.22

The MVDR algorithm provides an adaptive beamforming solution that can achieve high resolution and better interference rejection compared to conventional delay-and-sum beamforming. It adapts the beamforming response based on the spatial characteristics of the received signals, making it suitable for applications such as wireless communication systems, radar systems, and sonar systems.

Although the MVDR algorithm is very useful, it can be sensitive to errors in the covariance matrix estimation, especially when the number of snapshots (samples) is limited. Efforts have been made to develop robust versions of the MVDR algorithm to mitigate these issues, such as the Subspace-based MVDR (SMVDR) [10] and the Recursive MVDR (RMVDR) algorithms [11].

Additionally, the MVDR algorithm is susceptible to errors in the steering vectors calculations. Due to the sensitivity of electromagnetic signals, the calculations of the steering vectors can assume some errors. Research has been conducted on optimal steering vector estimation to increase the accuracy of the steering vectors as well [12]

3.4: The LCMV Beamforming algorithm

The Linearly Constrained Minimum Variance (LCMV) beamforming algorithm is a widely used technique in adaptive antenna arrays to achieve spatial filtering and beamforming. It aims to maximize the signal-to-interference-plus-noise ratio (SINR) by optimally adjusting the weights of the antenna array.

The LCMV algorithm considers both the desired signal and interference sources to create a beam that maximizes the desired signal power while minimizing the power of interference and noise. It does this by imposing constraints on the array response. It works very similar to the MVDR algorithm, however, there is a constraint matrix imposed that can identify target and jamming signals

The LCMV works as follows [13]:

Array Geometry and Steering Vector: The LCMV algorithm assumes an array of antennas with known positions and a desired signal arriving from a specific direction. The array geometry and the steering vector, which represents the direction of arrival (DOA) of the desired signal, are essential inputs to the algorithm.

1. **Covariance Matrix Estimation:** The algorithm estimates the covariance matrix of the received signals at the antenna array. The covariance matrix represents the statistical properties of the received signals and is used to calculate the weights for the beamforming.
2. **Constraint Matrix:** The LCMV algorithm incorporates constraints to minimize the interference and noise while maximizing the desired signal power. These constraints are typically derived based on the desired signal and interference characteristics. The

constraint matrix defines the desired signal response and the nulling response for the interference.

3. **Weight Calculation:** The algorithm calculates the optimal weights for the antenna array by solving an optimization problem. The objective is to minimize the output power while maintaining the desired signal response and nulling the interference.
4. **Beamforming and Signal Reconstruction:** Once the optimal weights are obtained, the LCMV algorithm applies these weights to the received signals from the antennas to create a beam that enhances the desired signal and suppresses the interference. The beamformed signal is then reconstructed for further processing or transmission.

When compared the MVDR algorithm, the LCMV is extremely similar, except for one key aspect: the constraint matrix. The constraint matrix provides better interference rejection capabilities compared to other beamforming techniques like conventional delay-and-sum beamforming. However, it is computationally more complex due to the optimization process involved in weight calculation due to the extra constraint matrix.

The LCMV algorithm is commonly used in applications such as wireless communication systems, radar systems, and sonar systems, where the suppression of interference and noise is crucial for improved signal detection and estimation. Following [13], we can represent the optimal weights, w, as an optimization problem that is mathematically represented as:

$$min\ \boldsymbol{w^H R w}$$

$$s.t. \quad \boldsymbol{w^H a(r)} = \boldsymbol{g}$$

It is the same as the MVDR mathematical representation, except the solving the minimization problem via optimization techniques yields the solution:

$$\boldsymbol{w_{LCVM}} = \frac{\boldsymbol{gR^{-1}a(r)}}{\boldsymbol{a^{-1}}(r)\boldsymbol{R^{-1}a(r)}}$$

Equation 3.23

As mentioned earlier, it is extremely similar to the MVDR solution except that it is augmented by the restraint matrix $\boldsymbol{g}$. Similar to the MVDR beamformer, the LCMV algorithm can also be susceptible to errors in the covariance matrix estimation and the steering vector estimation.

3.5: Direction of Arrival (DoA) Estimation using MuSiC

In order for either the MVDR or the LCMV algorithm to work, the DoA (Direction of Arrival) of the signal must be known. In a real-world electromagnetic signal space, there is a high probability that the DoA is unknown. An example of this would be an adversary at an unknown location transmitting a jamming signal. However, using the MuSiC algorithm we can estimate the DoA's. The MuSiC algorithm was first detailed and discovered in 1973 by Pisarenko to estimate the frequencies that make up a complex sinusoid. Today, it is used in a vastly large number of DSP systems. One prominent area of research where the MuSiC algorithm is used is in adaptive antenna arrays. Pisarenko's original work is detailed in [14]. Much like MVDR and LCMV, the backbone of this work lies in the estimated covariance matrix, and more specifically, the eigen decomposition of the estimated covariance matrix. To start off, we will take a matrix representation of a received signal, calculate its covariance matrix, preform

the eigen-decomposition of the covariance matrix, and the orthogonality relationship between the signal and noise subspaces, to create a MuSiC spectrum.

Referring to [15] we can obtain the MuSiC Spectrum as follows. Consider the matrix representation of the received signal, X, below:

$$\boldsymbol{X}(\boldsymbol{t}) \;=\; a(\theta,\varphi)(S_{source}(t) + \; N(t))$$

$$\boldsymbol{X} \;=\; [X_1, X_2, \ldots, X_n]$$

In this case S is the representation of the source signal in its complex form is given as:

$$S_{source}(t) = \; A_{amp}(t)e^{j(f_c(t)\,+\Phi(t))}$$

Equation 3.24

a is the steering vector matrix composed of n steering vectors, which are referred to β, for each signal, and N(t) is the total noise received by all the array elements:

$$a(\theta,\varphi) \;=\; [\beta_1(\theta,\varphi), \beta_2(\theta,\varphi), \ldots, \beta_{n,}(\theta,\varphi)]$$

Equation 3.25

From calculating the covariance as follows:

$$\boldsymbol{R} \;=\; E[\boldsymbol{X}\boldsymbol{X}^H] \;=\; \boldsymbol{E}[\boldsymbol{a}\boldsymbol{S} + \; \boldsymbol{N}] \;=\; \boldsymbol{a}\boldsymbol{R}_{\boldsymbol{S}}\boldsymbol{a}^{\boldsymbol{H}} + \; \boldsymbol{R}_{\boldsymbol{N}}$$

Equation 3.26

Where $\mathbf{R_N}$ is the noise correlation matrix.

When eigen-decomposition is done to **R** it results in N (number of elements in array) number of eigen values out of which the larger F (number of signals) eigenvalues corresponds to

the signal sources and the remaining smaller N-F eigen values are related to the noise subspace. Now can represent R in eigenspace as:

$$\boldsymbol{R} = E[\boldsymbol{X}\boldsymbol{X}^H] = \boldsymbol{Q_S}\sum \boldsymbol{Q_S}^{\boldsymbol{H}} + \boldsymbol{Q_N}\sum \boldsymbol{Q_N}^{\boldsymbol{H}}$$

Equation 3.27

Where Qs and Q_N denote the basis for signal and noise subspaces. Since MuSiC exploits orthogonality, the following relationship holds true:

$$\beta^H(\theta,\varphi)(\boldsymbol{Q_N}) = 0$$

The Direction(s) of arrival can then be represented as of incident signal sources and the noise subspaces

$$\theta_{min} = argmin\ (\beta^H(\boldsymbol{Q_N})\boldsymbol{Q_N}^H\ \beta)$$

Equation 3.28

Finally, we can create the music spectrum by representing the above equation as its reciprocal

$$P_{Music} = \frac{1}{\beta^H(\boldsymbol{Q_N})\boldsymbol{Q_N}^H\ \beta}$$

Equation 3.29

A simple simulation was conducted in MATLAB for the MuSiC algorithm.

A simulated signal space was created where P = diag [|A1|2, |A2|2, ..., |AP |2] is the diagonal matrix of the signal powers and σ_w is the variance of the white noise, since this

algorithm takes uncorrelated noise into account. The covariance of the signal matrix was then estimated using equation 3.19. The angles of arrival were encoded in the steering vectors to be -55 and 55 degrees

After performing eigen-decomposition on the covariance matrix, we can create a frequency estimation function. It is also worth mentioning that R must be an MxM square matrix to exploit the eigenvalue/eigenvector decomposition. First, we can define the eigenvalue vector as $\lambda = [\lambda 1, \lambda 2, ..., \lambda M]$. The eigenvalue matrix is in descending order, so the largest eigenvalue is $\lambda 1$ and the smallest is λM. We can separate these into the signal subspace and the noise subspace where the eigenvalues corresponding to the signal subspace are $\lambda sig = [\lambda 1, \lambda 2, ..., \lambda P]$ and the eigenvalues corresponding to the noise subspace are $\lambda noise = [\lambda P + 1, \lambda P + 2, ..., \lambda M]$. The corresponding eigenvector matrices would be Vsig = [V1, V2, V3, ..., VP] and Vnoise = [VP + 1, VP +2, VP + 3, ..., VM] it can be shown in that. Finally, the MuSiC spectrum was calculated. Figure 3.2 is a plot of the angles of arrival.

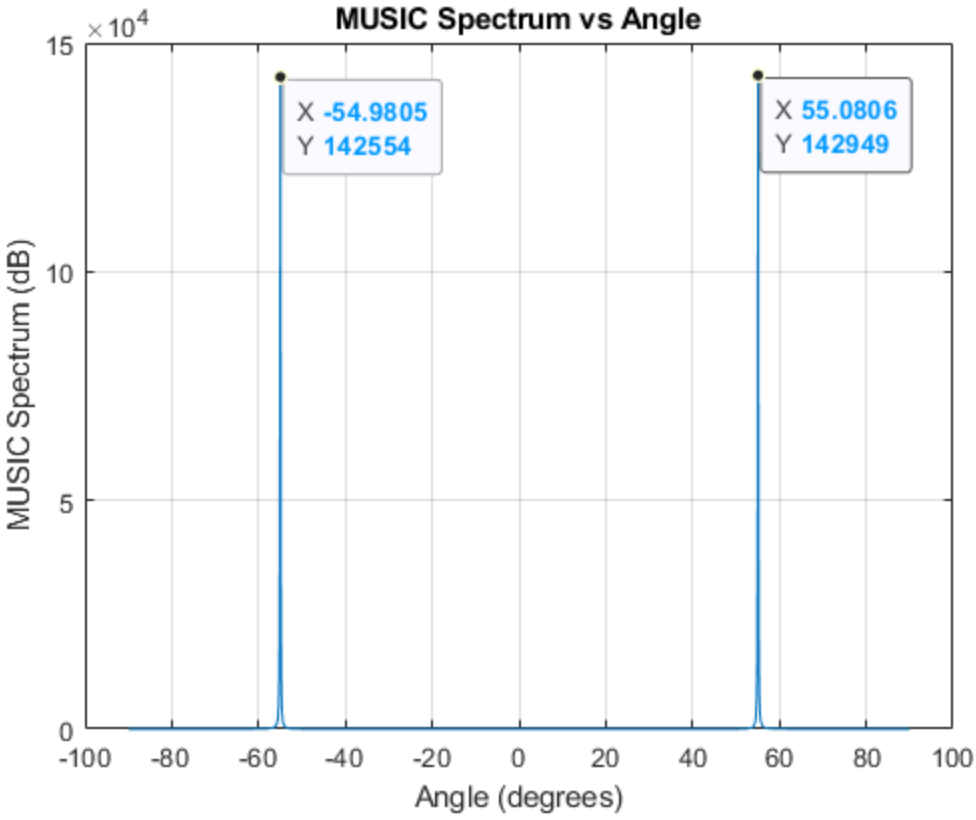

Figure 2.2: Simulated Angles of Arrival using MuSiC

As shown in Figure 3.2, the angles were estimated correctly within a small margin of error (0.036%). In a real-world application of anti-jam adaptive arrays, the MuSiC algorithm offers a robust and fairly simple way to extrapolate the directions of arrival from a received signal matrix and is extremely useful for users that do not the DoA of the incoming jamming signal. Note that there are other DoA estimation algorithms that are not included in this thesis, such as the ESPIRIT algorithm [16].

4. DESIGN OF GPS ANTENNAS

In this chapter, the design procedure for the antenna elements is outlined. There are 2 main constraints in the design of a GPS antenna as follows:

1. The design frequency of the antenna must be centered at the carrier frequency L1 (1575.52MHz)
2. The polarization of the antenna must be RHCP
3. The antenna bust have a relatively small bandwidth so only L1 is received.

Keeping these design constraints in mind, as well as the fabrication capabilities of the Antenna and RF Lab at The University of New Mexico, the “nearly square patch antenna” design was chosen.

4.1: The Nearly Square Patch Antenna

The nearly square patch antenna was realized by Lee [17]. In many cases, patch antennas can be fed with a power splitter of a coupler to obtain a required circular polarization. However, a more compact form of a circularly polarized antenna can be designed by splitting the fundamental operational mode into two degenerate modes that are equal in magnitude but 90 degrees out of phase (TM_{01} and TM_{10} modes). To split the fundamental mode into these two degenerate modes, a small perturbation is added, technically making the square patch a rectangular patch, but still close to the dimensions of a square, hence the name “nearly square.”

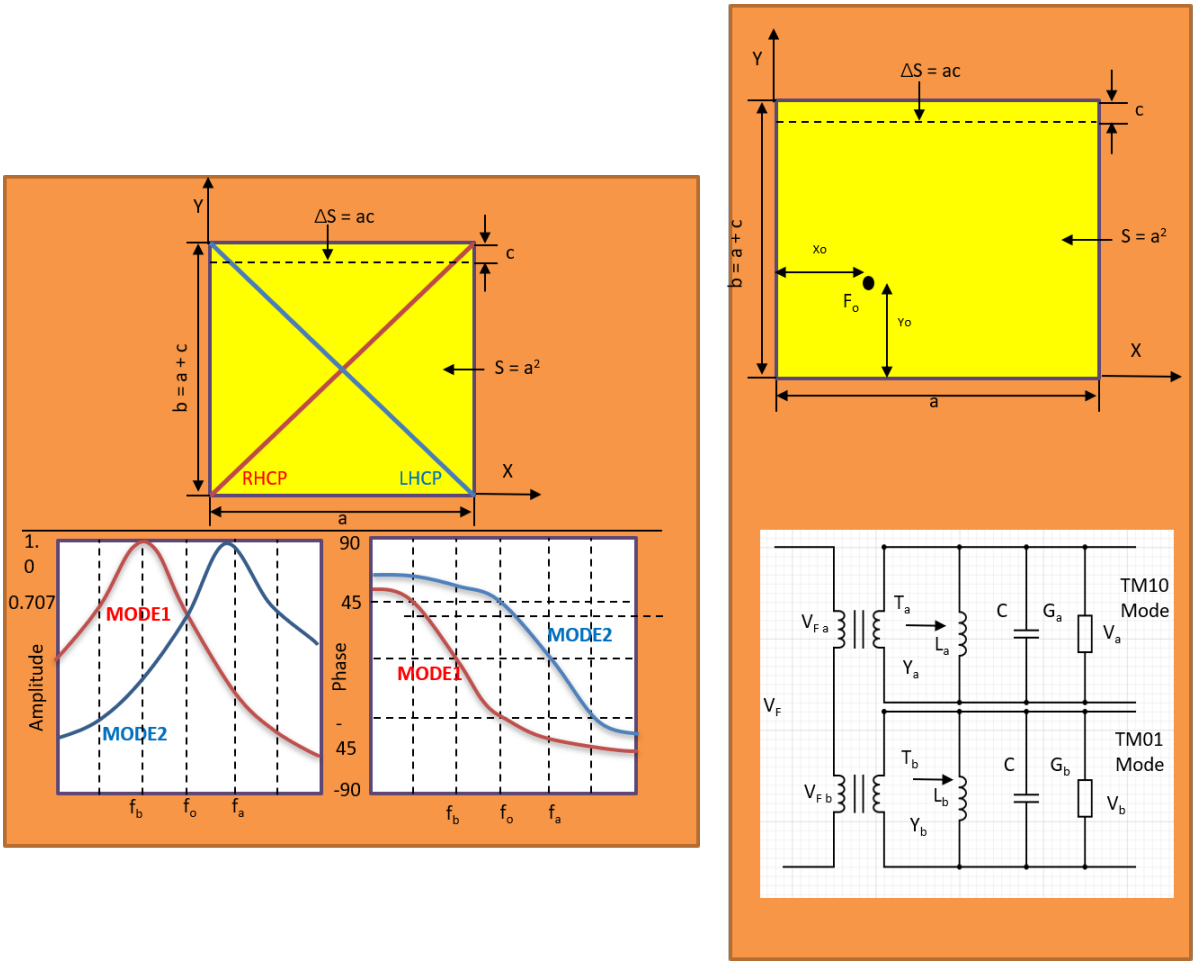

Figure 4-1: Nearly Square Operational Modes, Feed Location, and equivalent circuit

The radiation along the edges of the two degenerate modes are modeled by two equivalent circuits in the figure above. Circular polarization can be achieved by a probe feed along the RHCP or LHCP locus at a point (Xo,Yo). Given in [17], the ratio of turns of the two transformers can be given as:

$$\frac{Nb}{Na} = \frac{\cos\left(\frac{\pi Yo}{b}\right)}{\cos\left(\frac{\pi Xo}{a}\right)}$$

Equation 4.1

The turns ratio of the transformers is derived from the boundary conditions at the edges of the patch and is dependent on the feed location and the dimensions of the patch. Voltages along the edge of the patch can also be analyzed. For the TM10 mode, there is a voltage along the side of the patch. For the TM01 mode, there is a voltage Vb along the b side of the patch. In order to achieve CP, the proportion of the voltages along the edges must be equal in amplitude but with a 90-degree offset in phase. Realizing this, the proportion of the voltages can be given as:

$$\frac{Vb}{Va} = \frac{Nb}{Na} \times \frac{[\frac{fa}{Q} + j(fo - \frac{fa^2}{fo})]}{[\frac{fb}{Q} + j(fo - \frac{fb^2}{fo})]} = 1 \angle \pm 90^\circ$$

Equation 4.2

Where

fo is the design frequency.

fa and fb are the TM010 and the TM001 frequencies.

Q is the quality factor of the patch.

The frequencies for the two modes are given by:

$$fb = \frac{c}{2a_e\sqrt{\varepsilon_{reff}}}$$

$$fa = \frac{c}{2a_e\sqrt{\varepsilon_{reff}}}$$

Therefore:

$$\frac{fa}{fb} = 1 + \frac{\Delta Se}{Se}$$

We can then substitute in the above equation to into the CP condition and we get a magnitude and a phase solution. The magnitude condition is:

$$\alpha^4(r-1)+\alpha^2(rM^2-1)(\frac{1}{Q^2}-2)\ +\ rM^4-1\ =\ 0$$

Equation 4.3

And the phase condition is:

$$\alpha^4+\alpha^2(\frac{M}{Q^2}-M^2\ -\ 1)+M^2\ =\ \ 0$$

Equation 4.4

Where:

M = 1 + ΔSe /Se.

r = $(Nb/Na)^2$

α = fo/fb

Based on these conditions, a nearly square patch was designed at an operation frequency of L1. As mentioned previously, a nearly square patch antenna was chosen as the RHCP GPS antenna for this work due to the ease of manufacturing. The design philosophy taken for the nearly square was a combination of the process outlined in [18] and multiple CST Microwave Studio electromagnetic simulations. The substrate RO4003 with a dielectric constant of ϵr = 3.55 was chosen as our design substrate due to the ease of acquiring the material.

To start the initial design, a linearly polarized rectangular patch antenna was designed using the transmission line method described in [6]. In this method, an effective dielectric constant, and an extended length is calculated. This is done in order to compensate for fringing

effects the fields undergo at the edges of the patch antenna. GPS is a low enough frequency so the effective dielectric constant is essentially constant and can be defined as below:

$$\varepsilon_{reff} = \frac{\varepsilon_r + 1}{2} + [\frac{\varepsilon_r - 1}{2}][1 + 12\frac{h}{W}]^{-1/2}$$

Equation 4.5

And the equations for the design of the antennas extension length (ΔL), Length (L), and width (W) are as follows:

$$\Delta L = h(0.412)\frac{(\varepsilon_{reff} + 0.3)(\frac{W}{h} + 0.264)}{(\varepsilon_{reff} - 0.258)(\frac{W}{h} + 0.8)}$$

Equation 4.6

$$L = \frac{1}{2f_r\sqrt{\epsilon_o\varepsilon_{reff}\mu_o}} - 2\Delta L$$

Equation 4.7

$$W = \frac{1}{2f_r\sqrt{\epsilon_o\mu_o}}\sqrt{\frac{2}{\varepsilon_r + 1}}$$

Equation 4.8

Where h is the height of the dielectric. A simple rectangular patch was then designed for L1 in CST.

Following the design procedure in [7] the Q factor was determined from the simulated rectangular patch by looking at the impedance bandwidth of the linearly polarized patch. Since we were using a coaxial feed that comes through the back of the antenna, the parameter sweep function in CST was utilized. The feed location (both xo and yo) was swept in small increments of 0.1mm and the results with the best VSWR at L1 were chosen. The impedance bandwidth is defined as the range of frequencies where the antenna has good impedance matching. The industry standard for good matching is an S11 < -10dB (VSWR < 2). This standard was considered and the maximum VSWR was restricted to 2 when in the following equation:

$$BW_{LP}^{IMP} = \frac{VSWR_{max} - 1}{Q\sqrt{VSWR_{max}}}$$

Equation 4.9

After determining the Q, the rest of the design procedure from [18] was carried out and the length and width of the nearly square were solved for using the following relation:

$$\frac{W}{L} = \frac{2Q + 1}{2Q - 1}$$

Equation 4.10

From there another parameter sweep of the feed location was run to optimize the VSWR and the AR. The result was the final design for the nearly square patch antenna. Further quantitative results for the actual fabricated antenna are detailed in Chapter 5.

4.2: Jamming Power Levels of GPS

The power level of GPS signals received by antennas can vary due to factors such as satellite transmit power, satellite antenna gain, and atmospheric conditions. However, the typical power level of GPS signals received on Earth is in the range of -130 to -160 dBm at the receiver antenna. This can be confirmed by a GPS satellite link budget [19]. For reference, a link budget is a total summation that accounts for all power losses that the signal will experience in a telecommunication system. Due to the low receive power of GPS signals, GPS receiver front ends are deliberately designed to amplify the signal with minimum noise and filter out other frequencies.

On the other hand, GPS jammers are deliberately designed to emit radio frequency signals at power levels much higher than the GPS signals. The power levels of GPS jammers can vary widely, depending on the type and strength of the jamming device, as well as the intention (electronic warfare, illegal civilian jamming, testing, etc.) Some low-quality or consumer-grade jammers may have power levels around a few milliwatts (mW), while more powerful jammers used in certain situations, such as military or illicit activities, can reach power levels of tens or hundreds of watts (W).

4.3: Other Techniques and Challenges for Designing GPS Antennas

There has been quite extensive research on GPS antennas. In order to achieve a center frequency of L1, RHCP, and a sufficiently sized bandwidth, many techniques have been researched and implemented with regards to GPS antenna design.

Spiral and Helix antennas [2]:

Spiral antennas and helical antennas are particularly attractive for GPS because they provide a small mechanical space and desirable polarization as well as impedance matching. It radiated from the region within the spiral where the circumference is equal to one wavelength, and each arm is fed 180 degrees out of phase so when it radiates the currents at opposite points on each arm add in phase in the far field. Below is a figure detailing the geometry of a spiral antenna. Where the low operating frequency and the high operating frequency are as follows

$$F_{low} = c/2\pi R_2$$

$$F_{high} = c/2\pi R_1$$

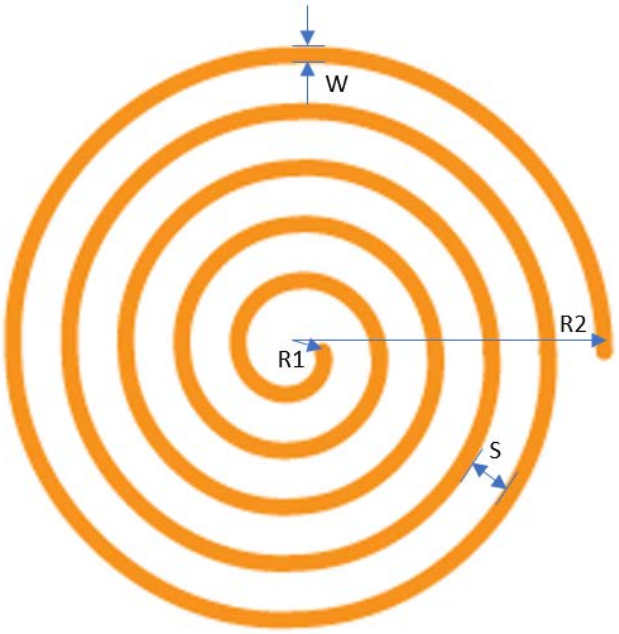

Due to the miniaturization of user devices and even performance degradation of the user and the environment, the design of GPS antennas is becoming more and more complex, and the following factors should be considered when designing for modern GPS antennas:

Limitation on the physical size:

A major technical limitation to GPS antennas comes from the shrinking size of modern devices. The space for mounting antennas on a PCB is really limited. One example of this can be seen on mobile devices. Antennas on mobile devices are generally linearly polarized in the form of planar inverted-F antennas and an LNA is generally used to combat the low gain of a linearly polarized antenna [1]. It is also worth mentioning that the advantages of CP antennas degrade in the presence of a multipath environment.

Multiband and broadband propagation:

Due to the multiple different GNSS services described in section 1 as well as the different frequency links, receivers need to be multiband in order to receive all frequencies necessary for the network. This is naturally a challenge since most small CP antennas are narrow band. Although this property is useful to block out interference, it also hinders the ability to receive multiple target frequencies.

The effects of the environment and human body:

The performance of a GPS antenna, or any antenna for that matter is greatly affected by its surroundings. Antennas can pick up multipath propagating signals through reflections and scattering of incident EM waves. In the vicinity of a human body, a well-known lossy media, the radiation efficiency, and therefore the gain can be reduced. If the device is surrounded by

metal, the faraday cage effect will take place and shield the receiving asset from all EM waves.

These three limitations pose significant design challenges for engineers and all have to be considered at different levels depending on the application.

5. SIMULATIONS AND FABRICATIONS

This chapter provides simulated results, fabrication techniques, and testing results. For the antenna, design parameters, electromagnetic simulation data and real-world electrical acceptance data are shown. For the algorithms used in the adaptive processing, MATLAB simulation results are provided.

5.1: Electromagnetic Simulations and Analysis of the Nearly Square Antenna

As mentioned in Section 4.1, to further tune and optimize the nearly square antenna, CST simulations were performed. The table below shows the parameters that were simulated and the results of the simulation that were deemed acceptable:

Parameters				**Results**		
Length (L)	Extension Length (c)	Feed location (xo,yo)	Line Impedance of Port @ Target Frequency	VSWR @ Target Frequency	Axial Ratio Boresight @ Target Frequency	Realized gain @ target frequency
48.55 mm	0.75 mm	(5.25,5.27) mm	49.822 Ohm	1.78	1.54 dB	5.4 dB

Table 2 CST Results and Parameters of Simulated Nearly Square Antenna

It is worth mentioning that to achieve these results, the parameter sweep option was used on the feed x and y coordinates of the feed location, as well as the extended width of the nearly square antenna. This assured for the most optimal simulated parameters. The figures below are some plots showing that the antenna was designed for L1, is in fact RHCP, has sufficiently large gain, and has sufficiently low bandwidth.

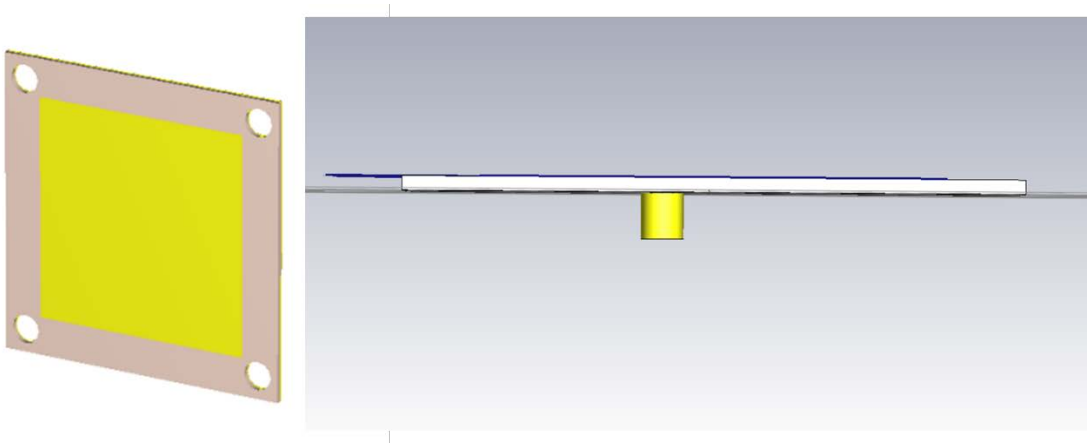

Figure 5-1: Nearly Sqare Patch CST model

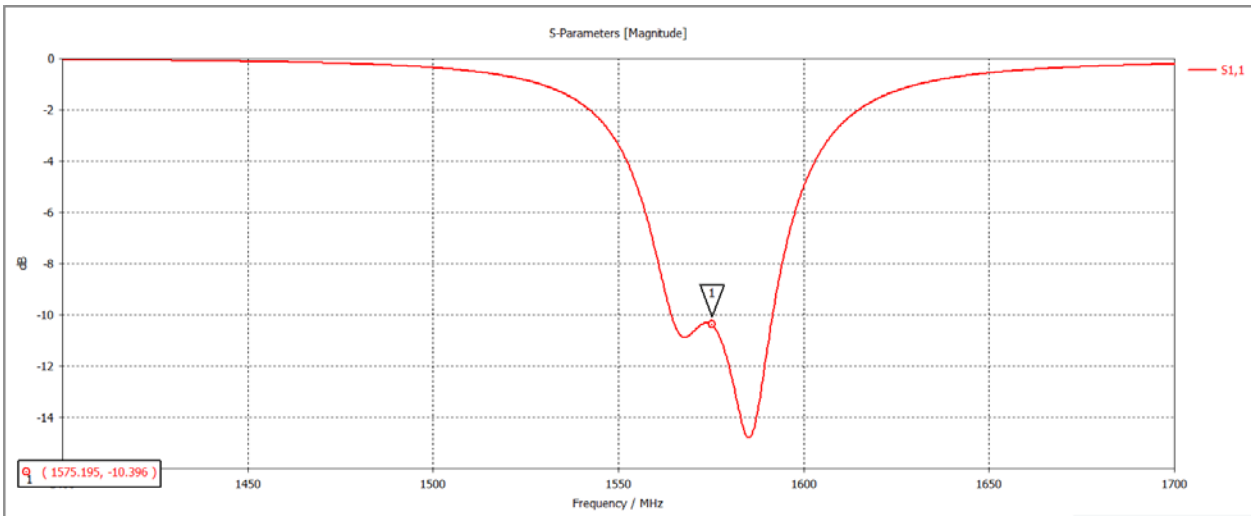

Figure 5-2: Nearly Square Patch Simulated Reflection Coefficient

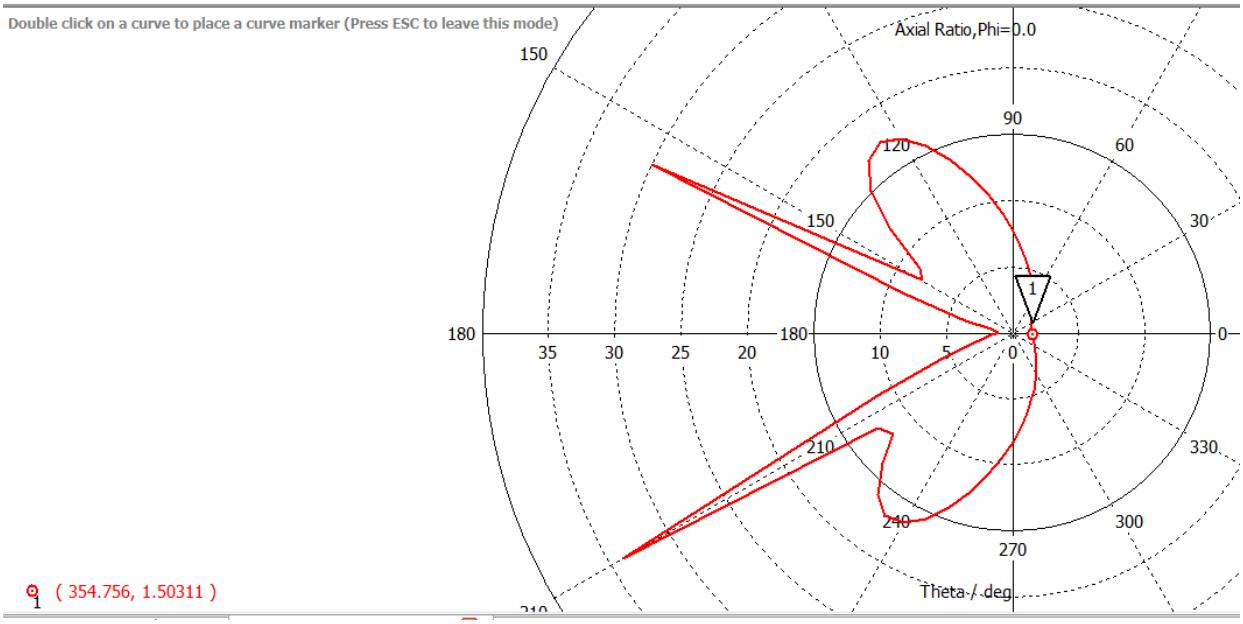

Figure 5-3: Nearly Square Patch Simulated Axial Ratio

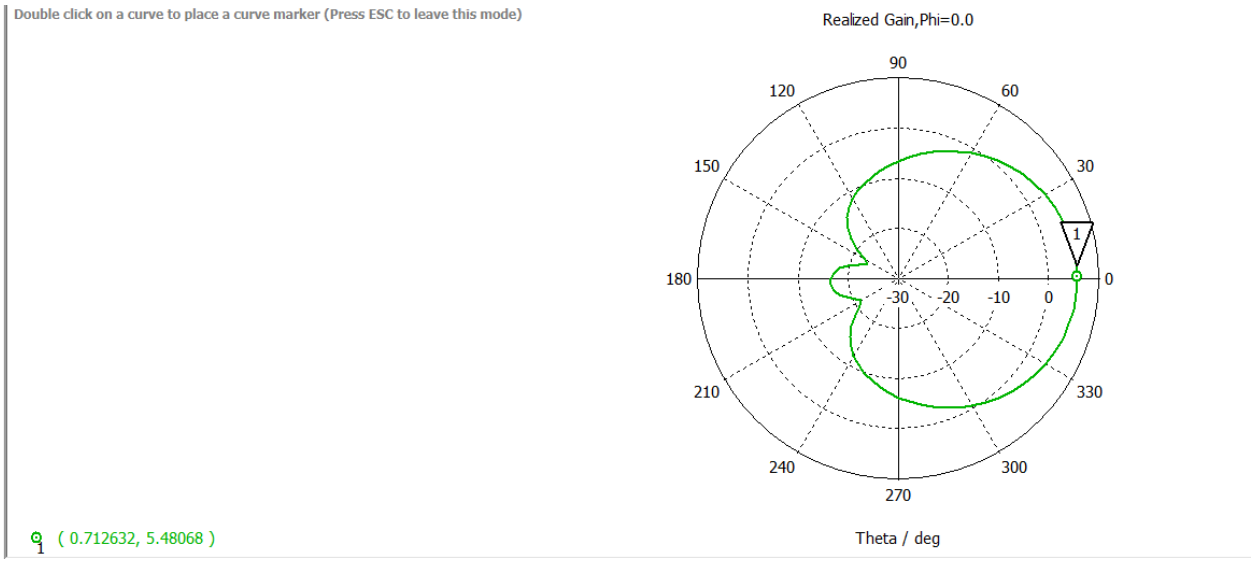

Figure 5-4: Nearly Square Patch Simulated Reflection Realized Gain

Figure 5-1 shows the CST model for the designed nearly square patch. Figures 5-2, 5-3, and 5-4 show the antenna's reflection coefficient, axial ratio, and realized gain, respectively

5.2: Fabrication of the Nearly Square Antenna

The nearly square GPS antenna was fabricated using an LPKF milling machine. A Rodgers material called RO4003C was used. 7 total antennas were fabricated. 1 as a prototype, 4 as test units, and 2 were used as backup units. Furthermore, some Pasternack PE45139 SMA male solder attachment connectors were purchased to be used as our coaxial probe connection.

The units were fabricated with an estimated engraving tolerance of ±0.3, which is acceptable for our design. Four ¼20 screw holes were also drilled on the corners of the ground plane so nylon screws can hold the antenna in position. For a ground plane a 12" x 12" sheet of aluminum was chosen. Screw holes were drilled into it that would hold each antenna in position. Multiple sets of screw holes were drilled for each array orientation. This design choice was made so the antenna array can be reconfigurable. In order to change the orientation of the array, the

nylon screws were manipulated according to the geometry of each orientation. Copper tape was used to cover up the screw holes that were not in used at the time of the test. Nylon screws were chosen over metal screws in order to avoid RF reflections, thus maximizing the performance of the antenna in a test scenario.

A few post-milling modifications were made to the antenna for the antenna to be usable.. The length of the SMA solder on probes needed to be shortened so they fit the antennas thickness. In order to do this, the probes were cut, and filed down with high grit sandpaper. It is important to note that this does not change the impedance of the probe, since the impedance of a coaxial is not dependent on length of the line, but rather the diameter of the conductors and dielectrics.

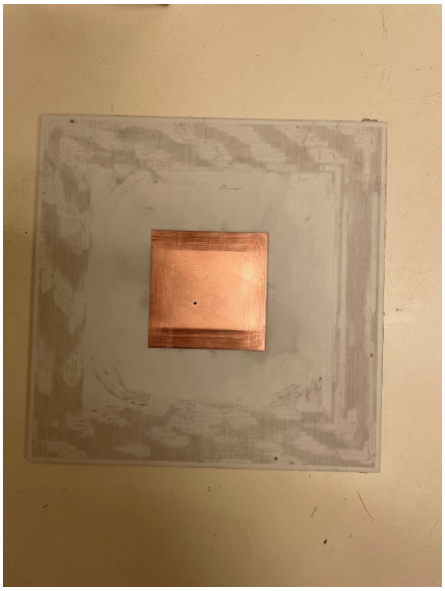

Figure 5-5: Prototype of Nearly Square Patch

As a figure of merit test, each antenna was taken to the roof of UNM's ECE building and tested by hooking it to a Keysight FieldFox in GPS receiver mode. In the GPS receiver mode, the FieldFox projects the latitude and longitude of its location AND locks on to the satellites it is using to determine the location. All 7 of the antennas passed this figure of merit test.

It is worth mentioning that each antenna had a RHCP gain of over 5dBi, but the AR was not always below 3dB. Although it is an industry standard to limit CP antennas to a 3dB AR, the designed antennas in this work did not meet that specification. However, the antennas were deemed acceptable because of their ability to pass the FieldFox figure of merit test and lock on to satellites. Moreover, the emphasis of this work was not to optimize the antenna patch, but to investigate the effectiveness of an array where each element is the same.

Figure 5-6: Nearly Square Patch as Functioning GPS Antenna

5.3: Simulations of the Beamforming Algorithms

In this thesis, two orientations of arrays were tested. “Orientation 1” and “orientation 2,” as shown in Figure 5-7 below.

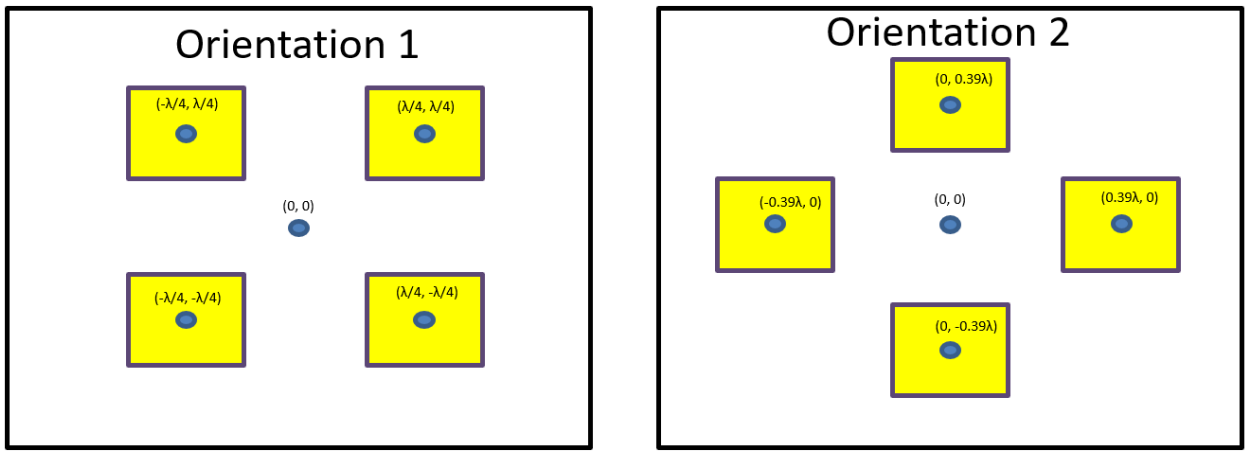

Figure 5-7: Geometry of Orientations

"Orientation 1" array is a simple a 2x2 square array with λ/2 spacing between each element. "Orientation 2" array is shifted by 45 degrees, resulting in a "+" shaped array. Optimally, Orientation 2 would have λ/2 spacing as well (λ/4 coordinates) however, we were limited by the size of the antennas, as the antennas elements would overlap on top of each other. As a result, a λ/2 spacing array in a "+" shaped array is not mechanically feasible. However, a 0.55λ spacing array is possible. This led to the above coordinates of the element locations. Due to the non-optimal spacing of orientation 2, grading lobes will be formed and the performance of orientation 2 will be sub-optimal [6].

As mentioned earlier, the two main beamforming algorithms used were the LCMV algorithm, and the MVDR algorithm on each orientation. Each algorithm was simulated in MATLAB prior to testing. The first goal achieved in the MATLAB simulations was to define the location of the target signal and the jamming signal. Although one could define any combination of θ and φ for each signal, a target signal coming in at $\theta_o = 0°$ $\varphi_o = 0°$ and a jamming signal coming in at $\theta_o = 60°$ $\varphi_o = 0°$ were chosen. These directions were chosen because it is simple to set up in an actual experiment. The steering vectors of each element had to be defined as below:

$$\mathbf{a}_r(\theta o, \varphi o)$$

$$= \left[e^{jk(dx_{r1}sin(\theta o)cos(\varphi o) + (dy_{r1}sin(\theta o)sin(\varphi o) + (dz_{r1}cos(\theta o))}, \ldots, e^{jk(dx_{rn}sin(\theta o)cos(\varphi o) + (dy_{rn}sin(\theta o)sin(\varphi o) + (dz_{rn}cos(\theta o))}\right]$$

Equation 5.1

We can then create a steering vector matrix as follows.

$$\boldsymbol{SV} = \begin{bmatrix} \boldsymbol{a\_target} \\ \boldsymbol{a\_jammer} \end{bmatrix}$$

Using these defined steering vectors is how the direction of arrival was encoded, where θo and φo were simply set to the directions of arrival mentioned above (θo = 0° φo = 0° for the target, and θo = 60° φo = 0° for the jammer.). The spatial positions of the antennas and the element index were also accounted for in the steering vectors by changing the (dx_{rn},$dy_{rn,}$ dz_{rn}).

A random BPSK signal with added random noise was then also created (using MATLABS "randn" function) and multiplied by the steering vector matrix and to get a simulated received signal. This math can be seen below as the received signal is defined as

$$\textbf{Received\_Signal} = \boldsymbol{SV} * (\boldsymbol{Rand\_BSPK\_Signal} + \boldsymbol{Noise})$$

This received signal had the same number of samples (time snapshots) that we planned to collect during actual testing, which was 1024.

From, there a covariance matrix was calculated based on the received signals using the equation:

$$\boldsymbol{R} = \frac{\boldsymbol{XX^H}}{1024}$$

The MVDR and LCMV weights were then calculated:

$$\boldsymbol{w_{MVDR}} = \frac{\boldsymbol{R^{-1}a(r)}}{\boldsymbol{a^{-1}(r)R^{-1}a(r)}}$$

$$\boldsymbol{w_{LCMV}} = \frac{\boldsymbol{gR^{-1}a(r)}}{\boldsymbol{a^{-1}(r)R^{-1}a(r)}}$$

For the LCMV case, a constraint matrix was used that constrained the first signal (at θo = 0° φo = 0°) to the target and the second signal (θo = 0° φo = 60°) to the jamming signal.

g = [1 0]

A "complete spectrum response" was also calculated that gave the effective radiation pattern of the array for every angle of θo and φo. This "complete spectrum response" depends on the array's element positioning and their effective radiation pattern. It was calculated mathematically determining steering vectors at each angle and antenna. Since the steering vectors represent the set of phase-delays for an incoming wave at each sensor element, multiplying them by the weighting matrix will effectively give us a normalized radiation pattern.

$$\boldsymbol{R}(\theta\ \varphi) = \boldsymbol{w}\,\boldsymbol{a}(\theta, \varphi)$$

It is important to note that all the weights in the weighting matrix must add up to 1 for the normalized pattern, and when all the weights are equal, the pattern is the "quiescent" radiation pattern. This means that there is no adaptation and the radiation pattern is the same as a radiation pattern without any weighting. If it was pertinent to change the simulated position of the antennas in the array, one would simply change the cartesian coordinates when defining the steering vectors for each antenna.

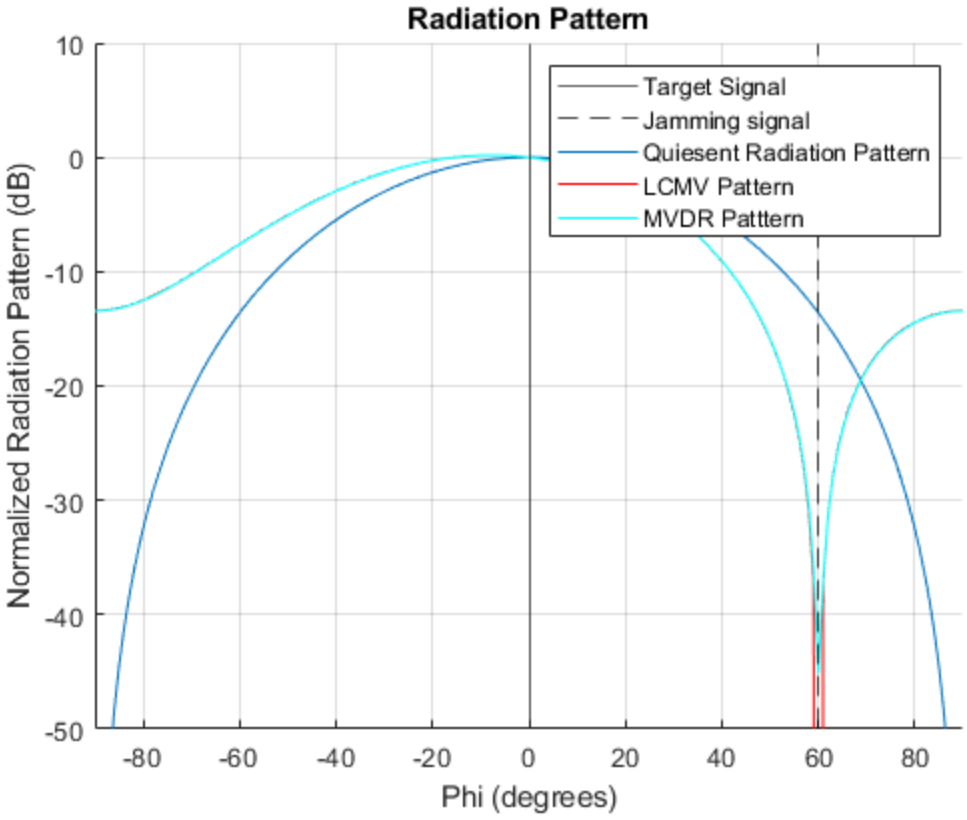

Figure 5-8: Simulated Radiation Pattern @ $\theta = 0$

Figure 5-8 shows a slice of the radiation pattern at $\theta = 0°$. The quiescent pattern looks like as expected for a 2x2 square array with $\lambda/2$ spacing: A "bulb" with a peak in the middle. Furthermore, the adaptive patterns (LCMV and MVDR) are beam nulling at the correct location. The target signal is received at max, while the jamming signal at $\varphi = 60°$ is nulled out.

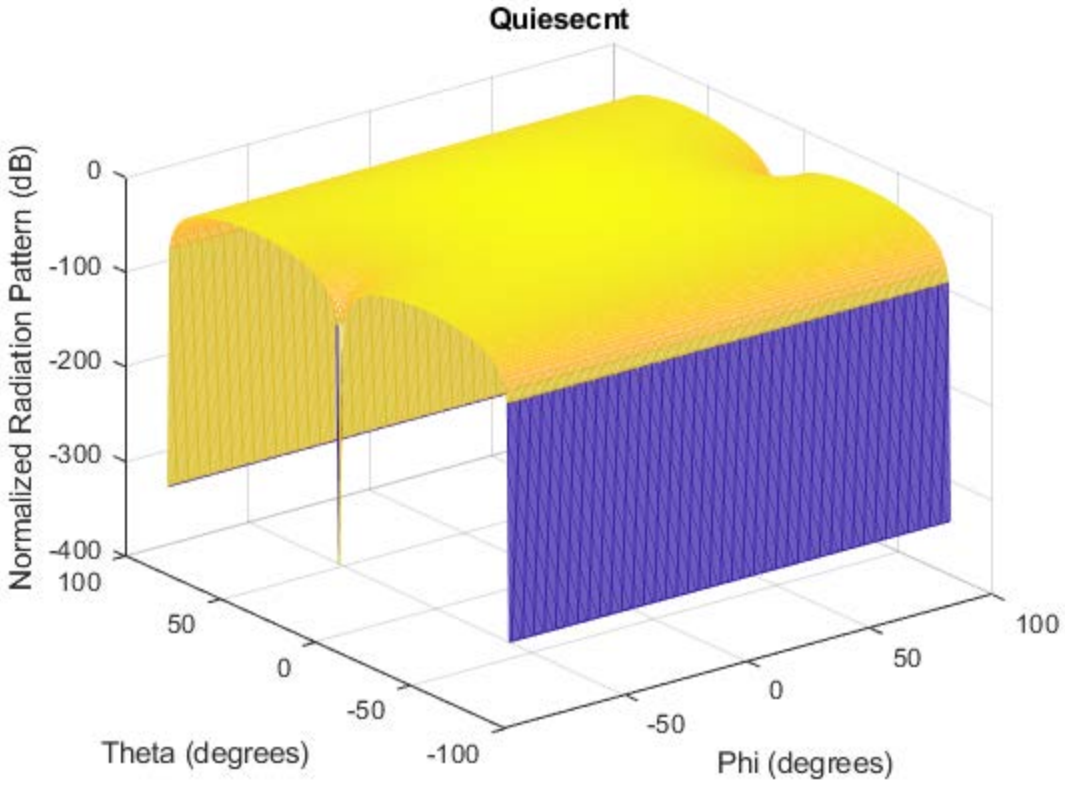

Figure 5-9: Simulated Quiescent Radiation Pattern

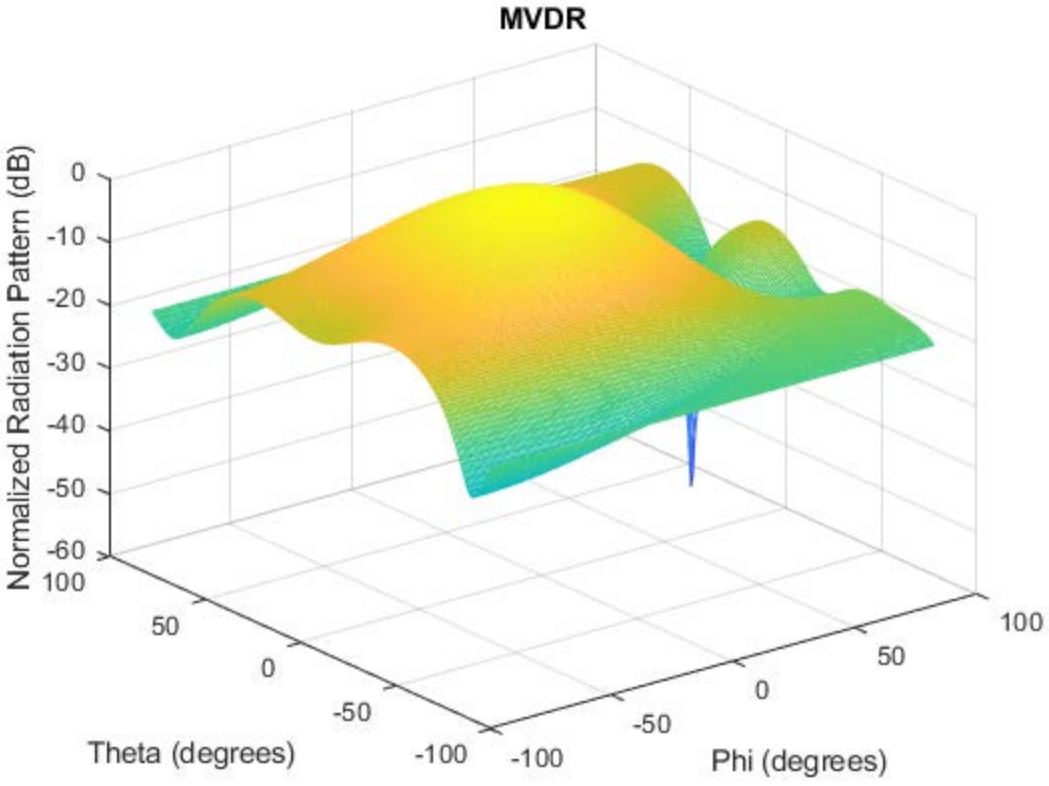

Figure 5-10: Simulated MVDR Radiation Pattern

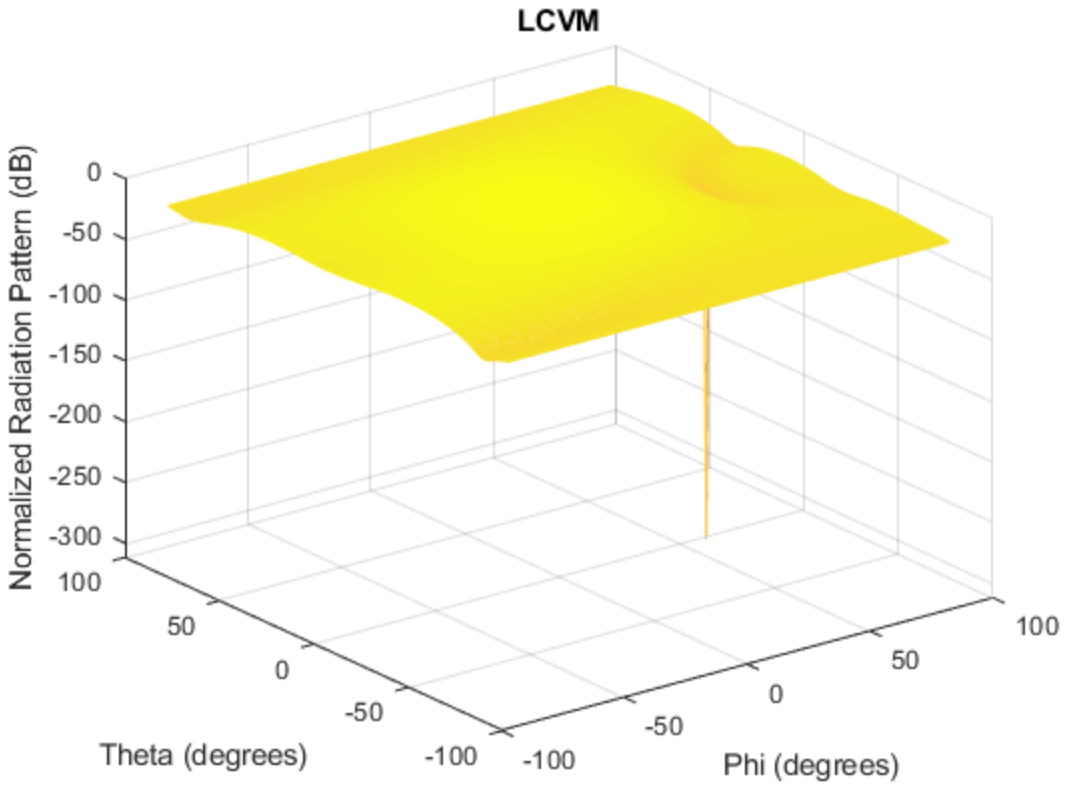

Figure 5-11: Simulated LCMV Radiation Pattern

Figures 5-9, 5-10, and 5-11 show the complete radiation pattern for "Orientation 1" for the quiescent pattern, the MVDR pattern, and the LCMV pattern respectfully. Each of the beam nulling algorithms nulls at the correct location ($\theta o = 0°$ $\varphi o = 60°$). The quiescent pattern also looks as expected.

6. EXPERIMENTAL SETUP AND RESULTS

In this chapter, the experimental test setup is described, and the results are shown and discussed. Also, the SDR (Software Defined Radio) platform used to apply the beamforming is discussed in detail. The hypothesis is simple: due to the non-optimal spacing of Orientation 2, Orientation 1 will outperform Orientation 2.

6.1: Analog Devices FMCOMM5 Software Defined Radio.

Figure 6-1: FMCOMM5 Software Defined Radio

In order to apply beamforming, a way must be devised to capture the signals, apply the weighting mathematics to create the adaptive signal, and transmit an adaptive signal. The received signals at each antenna are captured and put into a matrix, imported into a computer that does the necessary mathematics to create the adaptive signal vector, and finally transmitted out to a signal analyzer/GPS receiver. In order to do this, the Analog Devices FMCOMM5 Software Defined Radio board was utilized, as shown in Figure 6-1. This SDR was chosen for multiple of reasons. First, it has 4 receive ports and 4 transmit ports. Although only one transmit port was required to transmit the adaptive signal, all 4 receive ports were needed to receive the signal at each antenna. Second, the FMCOMM5 frequency covers the L1 frequency of interest. Finally, the FMCOMM5 has python wrappers for remote control and programming. A python script was

written to capture the total signal coming in, apply the beamforming, and transmit out the adaptive signal.

The fact that the FMCOMM5 and most SDR's are limited to 4 Rx ports was the limiting factor in this thesis regarding the number of planar elements that could be used. A 4-element design was chosen to match the number of Rx ports most SDR's have.

6.2: Experimental Setup

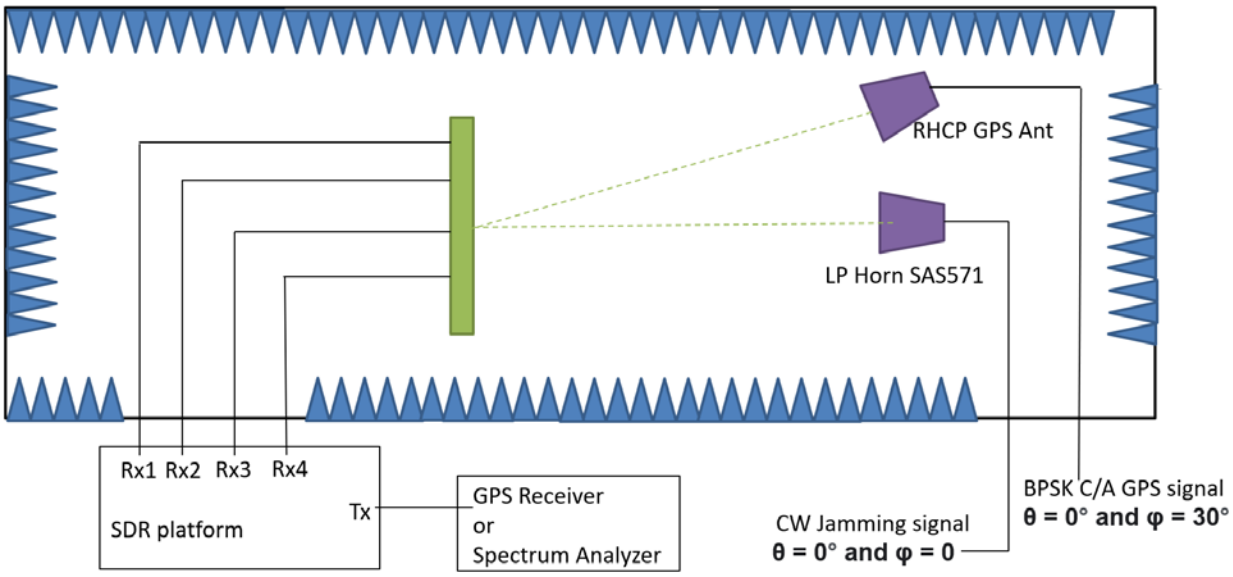

Figure 6-2: Experimental Setup

Figure 6.2 outlines the experimental setup. It consists of the array in the WW1 anechoic chamber with a jamming signal at (θo = 0° φo = 0°) and a target signal at (θo = 0° φo = 30°). The antenna array fabricated recorded the incoming signal, applied the beamforming with the FMCOMM5 SDR, and sent the signal to a GPS receiver/ Spectrum analyzer to record the power.

The test matrix is shown in table 3:

	GPS receiver Data			Spectrum analyzer power @L1		
	MVDR	**LCMV**	**Quiescent**	**MVDR**	**LCMV**	**Quiescent**
Orientation 1	✔	✔	✔	✔	✔	✔
	✔	✔	✔	✔	✔	✔
Orientation 2	✔	✔	✔	✔	✔	✔
	✔	✔	✔	✔	✔	✔

Table 3: Original Test Matrix

Sandia labs have what is known as a GPS link at the top of their buildings. The GPS link is just a GPS antenna that receives GPS signals, and coaxial cables that run through the buildings. In order use the signal in any of the labs. This GPS link was used to capture a real GPS signal for the experiment. Unfortunately, the GPS signal was much weaker than expected, and it was unable to be read in the chamber. This was due to the extra losses in the long coaxial cables running through the building. Since he anechoic chamber was only reserved for 3 days at Sandia Labs, there was not enough time to test the GPS receiver under jamming. As a result, we had to forgo the figure of merit GPS receiver test. The test matrix had to be modified as follows:

	Spectrum analyzer power @L1		
	MVDR	**LCMV**	**Quiescent**
Orientation 1	✔	✔	✔
	✔	✔	✔
Orientation 2	✔	✔	✔
	✔	✔	✔

Table 4: Modified Test Matrix

If the test matrix is completed, there should be sufficient results to quantitively compare the orientations to each other as well as the algorithms. The spectrum analyzer will be able to record the received power, and therefore give us a measurement proportional to cancellation.

To calibrate the SDR, a phase sync operation was implemented. This ensured that the phases were ONLY manipulated by the antenna locations and the beamforming algorithms, and not the SDR. In order to do this, the receive ports were connected to the transmit ports and the analog devices phase sync operation was followed in [20].

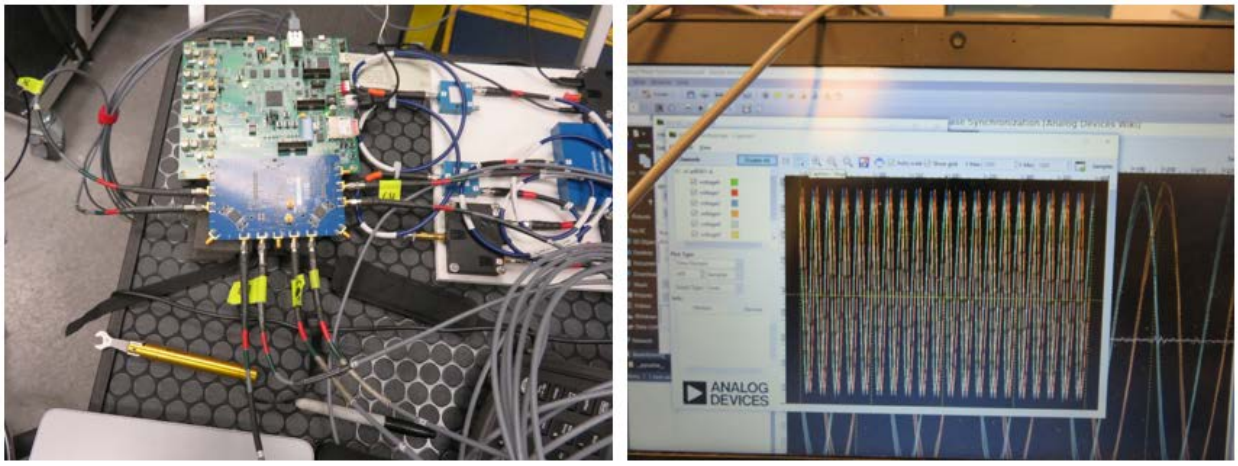

Figure 6-3: Phase Sync Set UP

From Figure 6.3, it can be seen that the phase sync operation was successful. Once the phase sync was completed the testing began and the test matrix was filled out. Figures 6.4 shows the antenna and the test set up in the anechoic chamber. In order to synthesize a jamming signal at L1, a Windfreak 10MHz to 15GHz RF Signal Generator was used. That was connected to the horn antenna at 0 degrees, and each of the antennas on the array were connected to the SDR. Figure 6-5 was included to better understand how each orientation looked on the ground plane.

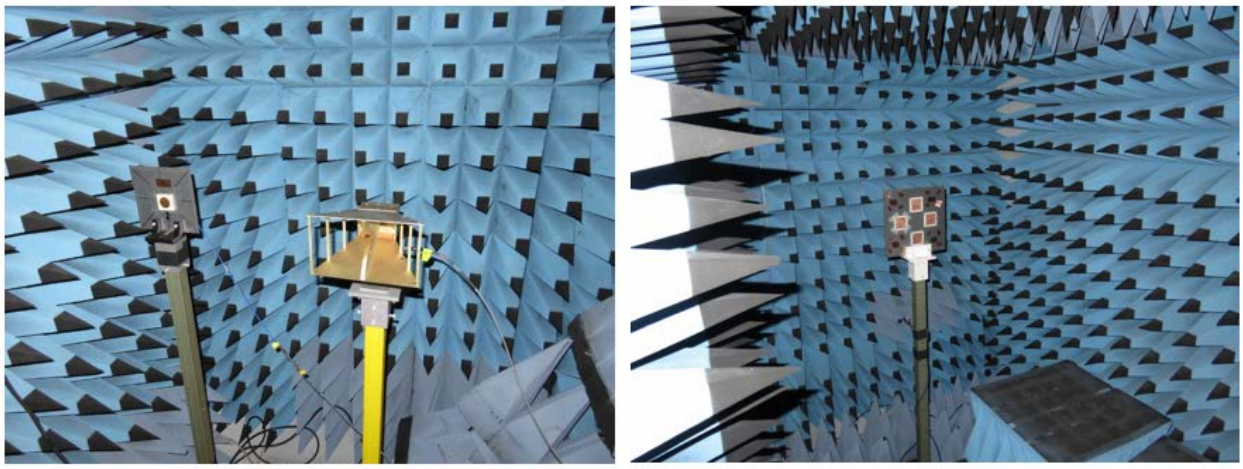

Figure 6-4: Photos of Experimental Set Up

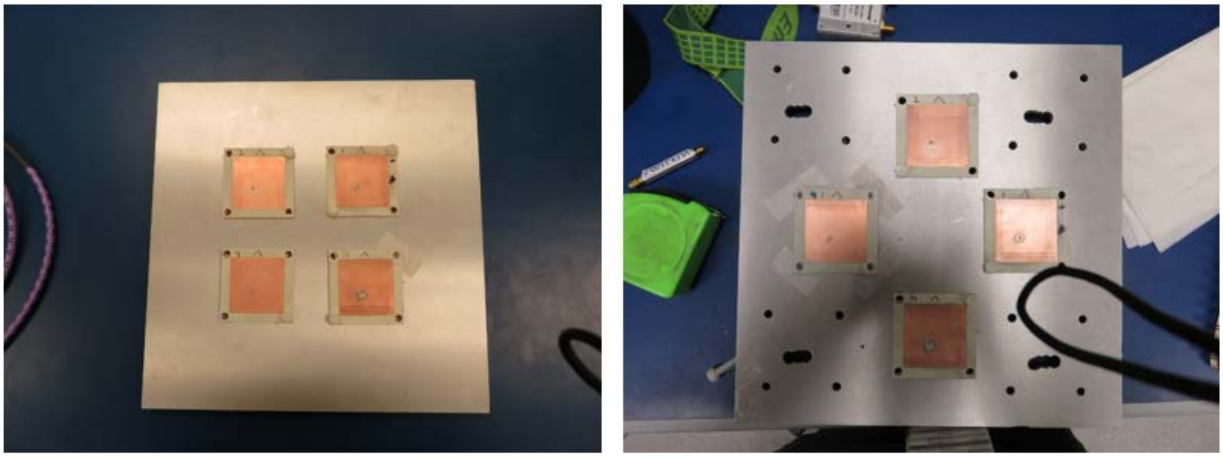

Figure 6-5: Photos of Orientation

6.3: Experimental Results

To reiterate, the INR and Cancelation of an adaptive beam nulling array can be described as follows:

$$\text{INR} = \frac{\boldsymbol{w^H R w}}{\boldsymbol{w^H w}}$$

$$C = \frac{INR(before\ adaptation)}{INR(after\ adaptation)}$$

And we can represent the cancellation in decibels as follows:

$$C_{dB} = 10\log(C)$$

The cancelation was calculated as the quantitative result comparing each algorithm and each orientation. Below in Figures 6-6 and 6-7 are the main results for Orientation 1 and 2 respectively. It outlines the covariance matrix of the received signal, the weighting for each algorithm and PSD for each algorithm

```
R =

   4.2468 + 0.0000i   4.0305 + 0.0295i  -1.7292 - 1.2754i  -1.7189 - 1.2562i
   4.0305 - 0.0295i   4.2324 + 0.0000i  -1.7729 - 1.2361i  -1.7525 - 1.2257i
  -1.7292 + 1.2754i  -1.7729 + 1.2361i   4.1896 + 0.0000i   3.9761 + 0.0226i
  -1.7189 + 1.2562i  -1.7525 + 1.2257i   3.9761 - 0.0226i   4.1573 + 0.0000i
```

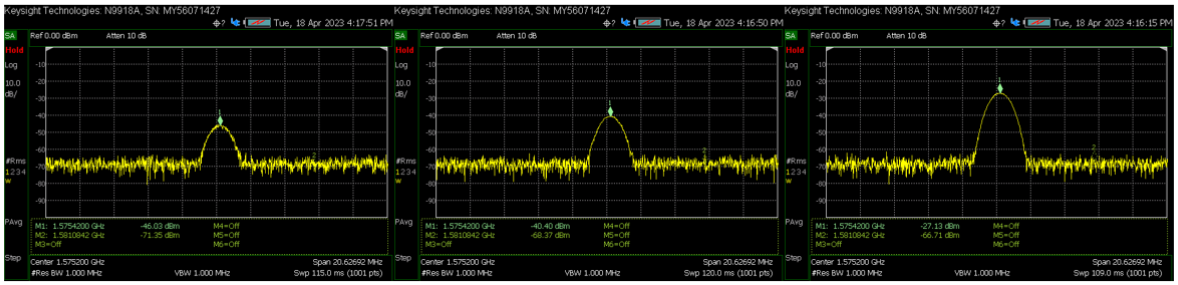

MVDR

```
w_mvdr =

   0.2108 + 0.0691i
   0.2864 + 0.0373i
   0.2493 - 0.0918i
   0.2535 - 0.0147i
```

LCVM

```
w_lcvm =

   0.2125 + 0.0689i
   0.2875 + 0.0379i
   0.2481 - 0.0919i
   0.2519 - 0.0149i
```

Quiescent

```
w_q =

   0.2500
   0.2500
   0.2500
   0.2500
```

Figure 6-6: Orientation 1 Results

```
R =

   1.0e+02 *

    1.1118 + 0.0000i  -1.3745 - 0.0664i   1.4900 + 0.4104i  -0.4122 + 0.5755i
   -1.3745 + 0.0664i   3.3154 + 0.0000i  -3.2638 - 0.6875i   0.8396 - 1.2830i
    1.4900 - 0.4104i  -3.2638 + 0.6875i   4.0155 + 0.0000i  -0.6396 + 1.6286i
   -0.4122 - 0.5755i   0.8396 + 1.2830i  -0.6396 - 1.6286i   1.4842 + 0.0000i
```

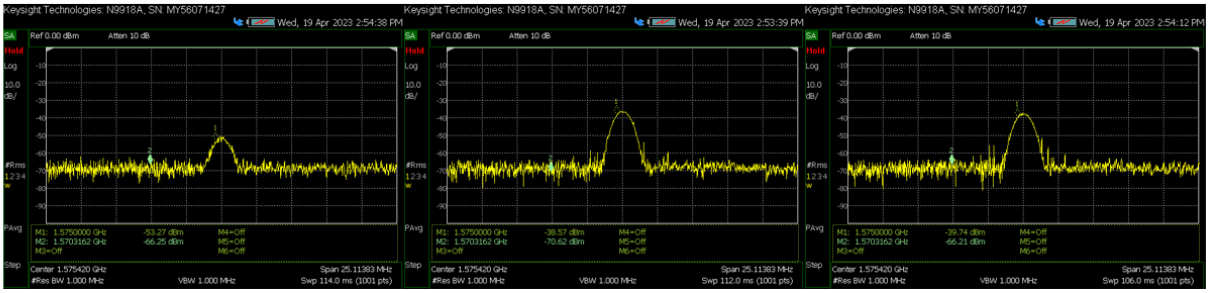

MVDR

```
w_mvdr =

   0.0597 - 0.1981i
   0.3021 - 0.0070i
   0.3342 + 0.0223i
   0.0573 + 0.1463i
```

LCVM

```
w_lcvm =

  -0.2292 - 0.4479i
   0.0789 - 0.0805i
   0.3065 + 0.1844i
  -0.1562 + 0.3440i
```

Quiescent

```
w_q =

   0.2500
   0.2500
   0.2500
   0.2500
```

Figure 6-7: Orientation 2 Results

		MVDR	LCMV	Quiescent
Orientation 1	**Spectrum Analyzer Power @L1**	-46.03 dBm	-40.40 dBm	-27.13 dBm
	Cancelation	38.76 dB	30.17 dB	0 dB
	INR (before)	-	-	482360
	INR (after)	62.9279	470.58	-
Orientation 2	**Spectrum Analyzer Power @L1**	-53.27 dBm	-38.57 dBm	-39.74 dBm
	Cancelation	3.6716 dB	2.3859 dB	0 dB
	INR (before)	-	-	80.1504
	INR (after)	34.2051	43.4706	-

Table 5: Final Results

Table 5 demonstrates that overall, the MVDR algorithm outperformed the LCMV algorithm, and Orientation 1 outperformed orientation 2. This confirms the hypothesis stated at the beginning of the chapter. Orientation 1 had a better cancelation value for both algorithms and received the overall signal better. Furthermore, the MVDR algorithm consistently had better cancelation values and received the jamming signal at less power.

7. CONCLUSION

In this thesis, the effectiveness of two anti-jam algorithms used on adaptive GPS antenna arrays was evaluated under different antenna element configurations. In this work, GPS signal

and GPS receiver front end architecture were presented and discussed. A literature review on adaptive antennas, the MVDR, and the LCMV beamnulling algorithms was conducted. A design for a nearly square GPS antenna was outlined and the antenna itself was fabricated, tested, and analyzed. Electromagnetic simulations were conducted and outlined on the nearly square antenna, and MATLAB simulations were performed on the MVDR and LCMV algorithms. Finally, an adaptive array with nearly square antenna elements was tested in an interference heavy environment, where a software defined radio hosting the MVDR/LCMV algorithms served as a beam nulling platform. Cancelation and received power spectral density were used as a figure of merit for measuring the effectiveness of the antenna arrays and the algorithms implemented.

7.1: Results Summary

The main contributions of this work envelop the world of antenna and RF engineering for interference mitigation. This work has:

1. **Created a reference and groundwork for the future development of adaptive antennas.**

   Jamming, whether it be intentional or not, is unfortunately a very common occurrence in GPS applications. Due to mechanical or spatial constraints, it is not always feasible to create a perfect planar array with half wavelength element spacing. The work in this thesis demonstrated how changing the elements spacing and phasing using different beamnulling algorithms can affect the way the cancelation of GPS jamming signals occurs, It is worth mentioning that prior to this work, there is very minimal research on how different phasing and spacing combinations effect these algorithms.

2. **Compared effectiveness of standard antenna element spacing to a less common + shape spacing.**

   The quantity defined by Fenn [7] referred to as cancelation is used as a figure of merit for the effectiveness for each antenna configuration (Orientation 1, an optimal 2x2 $\lambda/2$ spacing orientation, and Orientation 2, a less common "+" shaped array with 0.55λ spacing). Orientation 1 was up to 35 dB better in cancelation when compared to orientation 2.

3. **Compared effectiveness of LCMV and MVDR algorithm in single jammer signal space.**

   Although both algorithms have their advantages, in general, the MVDR algorithm preformed up to about 8dB better in cancelation applications compared to the LCMV algorithm.

4. **Provided background and a literature search on beamnulling and anti-jam adaptive antennas.**

   This work summarized the history and most important work regarding beamnulling and can be used as a quick guide in designing adaptive antennas for beamnulling.

7.2: Short Comings and Recommendations for Future Work

The short coming in this work was the failure to read an actual GPS signal. Optimally, results would have been provided that showed we were able to read a GPS signal when the jamming algorithms were deployed in an interference heavy environment. This failure was attributed to be because we lacked a proper 4 channel LNA in the receiver front end. As a result,

there were just too many losses in the system. In works such as [7], they encountered the same problem, but they were able to design a 4 channel LNA and the problem was mitigated. However, due to the fact that the test facility was unable to be scheduled in a timely manner again, the 4 channel LNA design was not tried. However, there is confidence that the antennas are able to receive GPS signals due to the fact that they worked outside.

Furthermore, more algorithms were initially planned to be tested and DOA estimation was planned to be implemented. However, due to the computational complexity of these algorithms, it was deemed that this would not be possible due to the SDR that was provided for this thesis. These more computationally complex beamnulling algorithms and DOA estimation algorithms require greater computational power than what the FMCOMM5 has to offer. Optimally, either a commercial beamformer or a designed beamformer would be used.

There is a large pool of future work that can be applied to this research. To list a few:

1. **Implement proper DoA estimation algorithms, so an unknown jamming signal direction can be nulled.**

As mentioned earlier in this thesis, the MuSiC [14] algorithm and the ESPIRIT [19] algorithm can be used to find the DoA of an unknown jamming source. Implementing this into the LCMV and MVDR algorithm will make it more effective against actual jamming sources, as the DoA information is usually not known, especially in cases of electronic warfare.

2. **Implement a “3D” array where elements are spaced in x y and z as opposed to a planar array (only x and y).**

Although this work was completed for a planar array design, a full 3D array can also de designed can be tested. This would allow for variation in the Z axis as well, that can possibly optimize the beamnulling and cancelation of the array.

3. **Enhance the accuracy of the steering vectors**

As mentioned earlier in this thesis research has been conducted on optimal steering vector estimation to increase the accuracy of the steering vectors as well [12]. This could a be a major source of error in in these algorithms, as all computations use the steering vectors of each antenna. By following the research in [12] more effective beam nulling can be implemented.

REFERENCES

[1] Anthony Flores, 14 May 2020, NAVSTAR Next Generation GPS Control Segment (OCX) to User Support Community Interface, ICD-GPS-870, 200 N. Pacific Coast Highway, El Segundo, CA 90245

[2] Chen X. Parini C.G. Collins B. Yao Y. Rehman M., Antennas for Global Navigation Satellite Systems, Wiley, 2012, West Sussex, United Kingdom, ch.1, sec.2.2, p.7

[3] Glennon E.P., Dempster A.G., “A review of GPS Cross Correlation Mitigation Techniques” 2004 International Symposium on GNSS/GPS, Sydney, Australia, December 2004

[4] Reed, I. S., “Brief history of adaptive arrays”, in IN: MILCOM '85 - Military Communications Conference, 1985, vol. 2, pp. 515–518.

[5] S. Applebaum, "Adaptive arrays," in IEEE Transactions on Antennas and Propagation, vol. 24, no. 5, pp. 585-598, September 1976, doi: 10.1109/TAP.1976.1141417.

[6] Balanis C.A., Antenna Theory: Analysis and Design 4e. Wiley, 2016, Hoboken, New Jersey, ch.6, sec.10.1, pp.348-354

[7] Alan Fenn. Adaptive Antennas and Phased Arrays for Radar and Communications, 2007.

[8] Monson H. Hayes. Statistical Digital Signal Processing and Modeling. 1st. USA: Wiley, 1996. isbn: 0471594318.

[9] Kiong TS, Salem SB, Paw JK, Sankar KP, Darzi S. Minimum variance distortionless response beamformer with enhanced nulling level control via dynamic mutated artificial immune system. Scientific World Journal. 2014; 2014:164053. doi: 10.1155/2014/164053.

[10] A. Pezeshki, B. D. Van Veen, L. L. Scharf, H. Cox and M. Lundberg Nordenvaad, "Eigenvalue Beamforming Using a Multirank MVDR Beamformer and Subspace Selection," in IEEE Transactions on Signal Processing, vol. 56, no. 5, pp. 1954-1967, May 2008, doi: 10.1109/TSP.2007.912248.

[11] M. -S. Chen and R. Liou, "Recursive MVDR for direction finding using circular arrays," 2004 10th International Symposium on Antenna Technology and Applied Electromagnetics and URSI Conference, Ottawa, ON, Canada, 2004, pp. 1-4, doi: 10.1109/ANTEM.2004.7860655.

IEEE Transactions on Signal Processing, vol. 56, no. 5, pp. 1954-1967, May 2008, doi: 10.1109/TSP.2007.912248.

[12] Yongwei Huang, Mingkang Zhou, and Sergiy A. Vorobyov. “New Designs on MVDR Robust Adaptive Beamforming Based on Optimal Steering Vector Estimation”. IEEE Transactions on Signal Processing, (July 2019), pp. 3624–3638. doi: 10. 1109 / 2019. 2918997.

[13] (2009). Linearly Constrained Minimum Variance Beamforming. In: Bourgeois, J., Minker, W. (eds) Time-Domain Beamforming and Blind Source Separation. Lecture Notes in Electrical Engineering, vol 3. Springer, Boston, MA. https://doi.org/10.1007/978-0-387-68836-7_3

[14] V. F. Pisarenko, The Retrieval of Harmonics from a Covariance Function, Geophysical Journal International, Volume 33, Issue 3, September 1973, Pages 347–366

[15] Pooja Gupta and S.P. Kar. “MUSIC and improved MUSIC algorithm to estimate direction of arrival”. In: (2015), pp. 0757–0761. doi: 10.1109/ICCSP.2015.7322593

[16] Paulraj, A.; Roy, R.; Kailath, T. (1985), "Estimation of Signal Parameters Via Rotational Invariance Techniques - Esprit", Nineteenth Asilomar Conference on Circuits, Systems and Computers, pp. 83–89, doi:10.1109/ACSSC.1985.671426, ISBN 978-0-8186-0729-5, S2CID 2293566.

[17] Sin Keng Lee, A. Sambell, E. Korolkiewicz, Shirt Fun Ooi and Yi Qin, "Design of a circular polarized nearly square microstrip patch antenna with offset feed," High Frequency Postgraduate Student Colloquium, 2004, Manchester, UK, 2004, pp. 61-66, doi: 10.1109/HFPSC.2004.1360353.

[18] Omer Can Dabak et al. “Interference Suppression in A GPS Receiver With 4element array design and Implementation of Beamforming Algorithms”. In: 2016 IEEE/ION Position, Location and Navigation Symposium (PLANS). 2016, pp. 645–652. doi: 10. 1109 / PLANS .2016.7479757

[19] Bhatti, Umar. (2013). Software based GPS receiver modules for a LEO satellite. 10.13140/RG.2.2.22138.90560.

[20] Getz, R. (2021, January 14). Wiki. FMComms5 Phase Synchronization [Analog Devices Wiki]. https://wiki.analog.com/resources/eval/user-guides/ad-fmcomms5-ebz/phase-sync